

Magnetic Field Strength and Spectral Distribution of Six Active Galactic Nuclei Jets

S. P. O’Sullivan¹ & D. C. Gabuzda¹

¹*Physics Department, University College Cork, Cork, Ireland*

Released 2008 Xxxxx XX

ABSTRACT

We use observations of six “blazars” with the Very Long Baseline Array (VLBA), at eight frequencies (4.6, 5.1, 7.9, 8.9, 12.9, 15.4, 22.2, 43.1 GHz), to investigate the frequency-dependent position of their VLBI cores (“core-shift”) and their overall jet spectral distribution. By cross-correlating the optically thin jet emission, we are able to accurately align the multi-frequency images of three of the jets (1418+546, 2007+777, 2200+420), whose core-shifts and spectra we find consistent with the equipartition regime of the Blandford & Königl conical jet model, where the position of the radio core from the base of the jet follows $r_{core}(\nu) \propto \nu^{-1}$. For the jet of 0954+658, we align the higher frequency images using our lower frequency measurements assuming equipartition in the radio core from 4.6–43 GHz. The jet emission of the other two sources in our sample (1156+295, 1749+096) is too sparse for our alignment technique to work. Using our measured core-shifts, we calculate equipartition magnetic field strengths of the order of 10’s to 100’s of mG in the radio cores of these four AGN from 4.6–43 GHz. Extrapolating our results back to the accretion disk and black hole jet-launching distances, we find magnetic field strengths consistent with those expected from theoretical models of magnetically powered jets.

Key words: radio continuum: galaxies – galaxies: jets – galaxies: magnetic fields

1 INTRODUCTION

Highly collimated jets of relativistic plasma are considered to be generated and propelled outwards from the central regions of Active Galactic Nuclei (AGN) by magnetic forces surrounding the supermassive black hole (see Meier 2009, and references therein). High resolution VLBI observations can detect the synchrotron emission from these jets in the radio regime at distances of the order of $10^3 - 10^7 r_g$, where $r_g = GM_{BH}/c^2$, corresponding to the sub-parsec to parsec scales of the jet (Lobanov 2006). Current theoretical models (Vlahakis & Königl 2004; Komissarov et al. 2007, hereafter K07) invoke rotation of the black hole magnetosphere and/or the inner accretion disk to create a stiff helical magnetic field that expels, accelerates and helps collimate the jet flow; an external medium is still required to confine the jet at its boundary, with a possible solution being a slower disk-driven wind outflow (e.g., Bogovalov & Tsinganos 2005). The models of Blandford & Rees (1974) and Daly & Marscher (1988) show how jets can be accelerated hydrodynamically, however, Königl (2007) proposes that extended acceleration regions are distinguishing characteristics of magnetohydrodynamic (MHD) dominated flows over purely hydrodynamical ones, and uses the model of Vlahakis & Königl (2004) to explain the parsec-scale acceleration of component C7 of 3C345 (Unwin et al. 1997).

In their conical jet model, Blandford & Königl (1979) [hereafter BK79] proposed that “the unresolved core be identified with the innermost, optically thick region of the approaching jet” with the base of the jet corresponding to the vertex of the cone. The radio cores of AGN generally have flat or inverted ($\alpha > 0$) spectra, where $S \propto \nu^\alpha$. The optical depth due to synchrotron self-absorption (SSA) is described by $\tau(r) \propto r^{(1.5-\alpha)m+n-1}\nu^{2.5-\alpha}$ (e.g., Rybicki & Lightman 1979), where m and n describe the power-law fall-off in the magnetic field strength ($B = B_{1\text{pc}}r^{-m}$) and particle number density ($N = N_{1\text{pc}}r^{-n}$), respectively, with distance from the central engine. Since VLBI resolution is usually not sufficient to completely resolve the true optically thick radio core, the core region contains emission from around the $\tau = 1$ surface at that frequency, as well as some contribution from the optically thin inner jet.

Furthermore, due to the frequency dependence of the $\tau = 1$ surface, the position of the radio core follows $r \propto \nu^{-1/k_r}$ (Königl 1981), where r is the distance from the central engine and $k_r = ((3 - 2\alpha)m + 2n - 2)/(5 - 2\alpha)$. For equipartition between the jet particle and magnetic field energy densities, the quantity $k_r = 1$, with the choice of $m = 1$ and

$n = 2$ being physically reasonable (e.g., Königl 1981; Hutter & Mufson 1986; Lobanov 1998a, hereafter L98), making k_r independent of the spectral index. Therefore, in equipartition, the “core-shift” ($\Delta r = r_{\nu_1} - r_{\nu_2}$) between two frequencies ($\nu_2 > \nu_1$) is directly proportional to $(\nu_2 - \nu_1)/(\nu_2\nu_1)$.

Since absolute positional information is lost during calibration of VLBI images, they are centered at the peak intensity of the map, which does not necessarily correspond to the furthest upstream component referred to as the VLBI core. For accurate combination of multi-frequency VLBI maps, we must properly align our images by correcting for the frequency-dependent position of the self-absorbed radio core. Phase-reference observations (Marcaide & Shapiro 1984) can be used to obtain the absolute position of the radio core by comparing the position of the target source with respect to a reference source, which should ideally be a point source, but this is a very calibration-intensive and weather dependent approach and gets much more difficult with observations at more than one frequency. The frequency dependent core-shift has generally been obtained by aligning model-fitted optically thin jet components at different frequencies (“self-referencing”) (e.g., Lobanov 1998a; Kovalev et al. 2008), but this method is unsuitable for smooth or weak jets that do not have a distinct component across a wide range of frequencies on which to align the images. An alternative method of aligning VLBI images is to cross-correlate the optically thin emission from the jet at multiple pairs of frequencies from regions where we do not expect large variations in the spectral index. Walker et al. (2000) used such a cross-correlation technique to successfully align his multi-frequency images of 3C84. We also use a cross-correlation technique for aligning our images, which involves comparing the optically thin jet emission at two frequencies with the highest correlation-coefficient occurring when the two images are best aligned; see Croke & Gabuzda (2008) for a detailed description of the method. From this method, we have been able to find reliable measurements for the frequency dependent core-shift of several sources across a wide range of frequencies (see O’Sullivan & Gabuzda 2008, for comparisons with both phase referencing and “self-referencing” methods).

From long-term monitoring of blazar jets, Marscher (2009) lists evidence supporting the idea that in some cases the cores correspond to a stationary feature such as a conical shock (Cawthorne 2006). He states that the core would correspond to either the $\tau = 1$ surface or the first stationary hotspot downstream of that surface, whichever is more intense at a particular epoch. Our core-shift measurements after the alignment of the multi-frequency images of 2200+420, 2007+777, 1418+546 and 0954+658 are consistent with the assumption of the

Table 1. Model Parameters for all sources

| Source | z | D_L (Mpc) | α_j | ϕ ($^\circ$) | Γ | θ ($^\circ$) | δ |
|----------|-------|----------------|------------|------------------------|-------------------|--------------------------|-------------------|
| 0954+658 | 0.368 | 1958 | -0.6 | 2.2 | 6.3* | 9.3 | 6.2 [†] |
| 1156+295 | 0.729 | 4481 | - | - | 25.1 [†] | 2.0 [†] | 28.5 [†] |
| 1418+546 | 0.152 | 716 | -0.5 | 1.9 | 4.5* | 11.2 | 5.1 [†] |
| 1749+096 | 0.320 | 1662 | - | - | 7.5 [†] | 3.8 [†] | 12.0 [†] |
| 2007+777 | 0.342 | 1797 | -0.5 | 1.0 | 8.0 | 7.2 | 7.9 [†] |
| 2200+420 | 0.069 | 307 | -0.5 | 1.9 [‡] | 7.0 [‡] | 7.7 [‡] | 7.2 [‡] |

Cosmology: $H_0 = 71 \text{ km s}^{-1} \text{ Mpc}^{-1}$, $\Omega_\Lambda = 0.73$ and $\Omega_M = 0.27$. Col. (1): IAU source name, Col. (2): redshift, Col. (3): luminosity distance, Col. (4): jet spectral index, Col. (5): jet half-opening angle, Col. (6): bulk Lorentz factor, Col. (7): jet viewing angle, Col. (8): Doppler factor. References: *Gabuzda et al. (1994), *Pushkarev & Gabuzda (1999), [†]Hovatta et al. (2009), [‡]Jorstad et al. (2005)

core corresponding to the $\tau = 1$ surface and not some stationary feature. It’s also worthwhile inspecting the core polarization because this can sometimes give information about scales smaller than the standard resolution at a particular frequency. From the polarization images of these sources presented in O’Sullivan & Gabuzda (2009), we do not see any clear evidence of distinct polarized features upstream of the total intensity core which would support the model of a stationary core feature through which ejected plasma blobs propagated.

In Section 2 we describe our observations and how we use our core-shift measurements to calculate magnetic field strengths. Our results for each source are presented in Section 3 and we discuss some of their interesting features in Section 4. Our conclusions are listed in Section 5.

2 OBSERVATIONS AND METHOD

Six “blazars” were observed on 2006 July 2 with the American Very Long Baseline Array (VLBA) at eight frequencies (4.6, 5.1, 7.9, 8.9, 12.9, 15.4, 22.2, 43.1 GHz) quasi-simultaneously (see O’Sullivan & Gabuzda 2009, for details). Here we present spectral index images for these six blazars along with estimates of the magnetic field strengths in the radio core from 4.6–43 GHz for four sources in which we were able to measure the “core-shift”. We follow the method described in L98 for calculating several important jet parameters from the frequency-dependent shift of the position of the VLBI core due to SSA. Table 1 lists the observed sources along with the model parameters used in our calculations.

Once our images are properly aligned, we generate spectral index (α) maps between pairs of frequencies in AIPS using the task COMB, with $\alpha = (\log S_{\nu_2} - \log S_{\nu_1}) / (\log \nu_2 - \log \nu_1)$ where S_ν is the measured flux at frequency ν . This approximates the spectrum as a straight line which should be a good approximation as long as there is not a spectral turnover

between the two frequencies. Spectral turnovers of components are often observed in VLBI jets (Lobanov 1998b) but useful information can still be extracted by generating maps from relatively closely spaced frequency pairs. In order to analyse the spectrum across our wide frequency range, we constructed spectral index maps from 4.6–7.9, 8.9–12.9, 15.4–22 and 22–43 GHz for each source. The images used to create each map have the same image size, pixel size and are convolved with the same beam, corresponding to the lower frequency of the pair. We also take a slice along the jet of each spectral index image for inspection.

Since the shift measurements from the cross-correlation program are found with respect to the Stokes I peak intensities, we use them in conjunction with the model-fitted core positions from `DIFMAP` (Shepherd 1997) to obtain the distance between the cores at different frequencies (“core-shift”). The task `UVRANGE` in `DIFMAP` was used to provide uv -ranges for the higher frequencies matching that of the lower frequencies when model-fitting. Due to the fall-off in the optically thin part of the synchrotron spectrum with increasing frequency and the large differences in resolution, aligning images across wide spacings in frequency can prove very difficult. However, with our excellent frequency coverage from 4.6–43 GHz, we are able to obtain many measurements from different frequency combinations which can be compared with each other to check for consistency.

To calculate the magnetic field strength with distance from the base of the jet, we combine the analysis of L98 and Hirotani (2005). The distance of the radio core from the base of the jet at the observed frequency ν in GHz, is given by

$$r_{\text{core}}(\nu) = \left(\frac{\Omega_{r\nu}}{\sin \theta} \right) \nu^{-1/k_r} \quad (1)$$

in parsecs, where θ is the jet viewing angle and $\Omega_{r\nu}$ is the core-position offset measure, defined in L98 as

$$\Omega_{r\nu} = 4.85 \times 10^{-9} \frac{\Delta r_{\text{mas}} D_L}{(1+z)^2} \left(\frac{\nu_1^{1/k_r} \nu_2^{1/k_r}}{\nu_2^{1/k_r} - \nu_1^{1/k_r}} \right) \quad (2)$$

in units of pc·GHz, where D_L is the luminosity distance in parsecs and Δr_{mas} is the measured core-shift in milliarcseconds.

We use the synchrotron self-absorption derivation for a conical jet by Hirotani (2005) and the equipartition condition, in cgs units,

$$N \gamma_{\text{min}} m_e c^2 = K \frac{B^2}{8\pi} \quad (3)$$

$$K = \frac{2\alpha + 1}{2\alpha} \frac{(\gamma_{\text{max}}/\gamma_{\text{min}})^{2\alpha} - 1}{(\gamma_{\text{max}}/\gamma_{\text{min}})^{2\alpha+1} - 1}. \quad (4)$$

where γ_{min} and γ_{max} are the low and high cut-offs of the electron energy distribution. Eval-

uating eqn. 43 from Hirotani (2005) for the simplified case $k_r = 1$ and $\alpha = -0.5$, we get the equipartition magnetic field in Gauss at 1 pc

$$B_1 \simeq 0.025 \left(\frac{\Omega_{r\nu}^3 (1+z)^2}{\delta^2 \phi \sin^2 \theta} \right)^{1/4} \quad (5)$$

where δ is the Doppler factor, θ is the viewing angle and ϕ is the half-opening angle of the jet. The magnetic field strength in the core at the observed frequency ν can then be found from

$$B_{\text{core}}(\nu) = B_1 r_{\text{core}}^{-1} \quad (6)$$

For spectral indices other than -0.5 , the magnetic field strength depends on the exact value of γ_{min} according to $B_1 \propto \gamma_{\text{min}}^{(2+4\alpha)/(7-2\alpha)}$. The dependence on K is much weaker since $\gamma_{\text{max}} \gg \gamma_{\text{min}}$. Equation 5 differs from the equipartition magnetic field at 1 pc derived in L98, eqn. 10, where our calculated magnetic field strengths are a factor of ~ 3 times smaller (e.g., compare our results for 2200+420 here with those in O’Sullivan & Gabuzda (2008)) due to the more accurate equipartition condition used in Hirotani (2005). Note that in all cases, where errors are presented, we have only considered the errors in the core-shift measurements.

3 MAGNETIC FIELD STRENGTH AND SPECTRAL INDEX RESULTS

3.1 2200+420 (BL Lac)

Fig. 1 shows the spectral index distribution for 2200+420 from 4.6–43 GHz. The core region displays a strongly inverted spectrum at low frequencies (Fig. 1a) before becoming less inverted at higher frequencies (Fig. 1b, c, d), consistent with SSA of emission from the unresolved part of the jet. Further downstream, the jet emission becomes optically thin, with the majority of slices consistent with a spectral index of ~ -0.5 . The direction of the slice along the core region in the 22–43 GHz map (Fig. 1d) follows the 43-GHz inner jet direction. There is an interesting feature in the 8.9–12.9 GHz map (Fig. 1b), at ~ 5 mas from the core, where the spectrum flattens considerably. This feature is also present in the 4.6–7.9 GHz and 15.4–22GHz maps, but is less pronounced, possibly due to the low resolution at 4.6 GHz and the lack of sensitivity to the extended jet emission at the higher frequencies. The presence of this feature might be due to some particle re-acceleration in the jet or interaction between the jet and the surrounding medium, since this is close to where the jet changes to a south-easterly direction in the plane of the sky.

The measured core-shifts for 2200+420 are listed in Table 2 along with the angle representing the direction of the shift measured from north through east. The average direction of the shift is $14 \pm 10^\circ$, where the error corresponds to the standard deviation, and this core-shift direction is consistent with the inner jet direction at 43 GHz of $\sim -163^\circ$. Table 3 lists the size of the shift as a fraction of the beamsize. Even though the shifts are only of the order of 5-20% of the corresponding beams, they still have quite a dramatic effect on the spectral index in the core if they are not taken into account.

Figure 2 shows each shift measurement, Δr , plotted against the expected frequency dependence for $k_r = 1$. The y-intercept from a straight line fit to the data is -0.01 ± 0.01 mas. From the slope of the line we determine a characteristic core position offset measure ($\Omega_{r\nu}$) of 3.4 ± 0.3 pc · GHz for 2200+420. Our results are also consistent with a previous core-shift estimate from Mutel et al. (1990) who found a shift of 0.3 mas between 5.0 and 10.6 GHz, corresponding to $\Omega_{r\nu} = 3.7$ pc · GHz (no error was presented with their result). Since the position of the core is expected to change with frequency according to $r_{\text{core}}(\nu) \propto \nu^{-1/k_r}$, observations at three or more frequencies enable determination of the parameter k_r . Our dense frequency sampling allows us to provide strong constraints on the value of k_r across our entire frequency range. Using 43 GHz as the reference frequency and averaging the various possible combinations of shift measurements (Table 3), we find our values to be consistent with a constant k_r of 0.99 ± 0.07 from 4.6–43GHz (Fig. 3). This indicates that the physical conditions in the compact jet region in 2200+420 do not change significantly between 4.6 and 43 GHz. A value of $k_r = 1$ indicates that the jet particle and magnetic field energy densities are in equipartition, and our derived value of k_r is consistent with this assumption.

Using our core-shift measurements, we can find estimates for the magnetic field strength, distance of the radio core to the base of the jet and the total jet luminosity. To do this we follow the method outlined in L98. Estimates of the jet opening angle, viewing angle, bulk Lorentz factor and Doppler factor are taken from multi-epoch VLBI observations of 2200+420 by Jorstad et al. (2005), see Table 1. These estimates are also consistent with more recent observations by Hovatta et al. (2009), who analyse the variability of radio flares from single dish measurements to obtain their jet parameters. We use a jet spectral index (α_j) of -0.5 for our calculations, consistent with our spectral index maps for this source (Fig. 1). We use the shift measurements listed in Table 2 to calculate the average core-position offset measure ($\Omega_{r\nu}$) from eqn. (2) at each frequency. Then for each $\Omega_{r\nu}$, we calculate

Table 2. All measured core-shifts for 2200+420, plotted in Fig. 2

| ν_1 (GHz) | ν_2 (GHz) | Δr (mas) | Angle ($^\circ$) |
|------------------|------------------|---------------------|-----------------------|
| 4.6 | 5.1 | 0.06 ± 0.07 | -1.0 ± 0.1 |
| 4.6 | 7.9 | 0.19 ± 0.07 | 15.2 ± 0.3 |
| 4.6 | 8.9 | 0.20 ± 0.07 | 15.5 ± 0.3 |
| 4.6 | 12.9 | 0.35 ± 0.07 | 19.4 ± 0.4 |
| 4.6 | 15.4 | 0.40 ± 0.07 | 16.3 ± 0.3 |
| 5.1 | 7.9 | 0.14 ± 0.07 | 22.0 ± 0.6 |
| 5.1 | 8.9 | 0.19 ± 0.07 | 16.4 ± 0.3 |
| 5.1 | 12.9 | 0.30 ± 0.07 | 23.3 ± 0.6 |
| 5.1 | 15.4 | 0.35 ± 0.07 | 19.1 ± 0.4 |
| 7.9 | 8.9 | 0.04 ± 0.04 | 5.6 ± 0.1 |
| 7.9 | 12.9 | 0.15 ± 0.04 | 18.8 ± 0.3 |
| 7.9 | 15.4 | 0.18 ± 0.04 | 14.0 ± 0.1 |
| 7.9 | 22.2 | — | — |
| 7.9 | 43.1 | 0.28 ± 0.04 | 6.4 ± 0.1 |
| 8.9 | 12.9 | 0.07 ± 0.04 | 11.0 ± 0.1 |
| 8.9 | 15.4 | 0.11 ± 0.04 | 20.9 ± 0.3 |
| 8.9 | 22.2 | 0.17 ± 0.04 | 13.1 ± 0.1 |
| 8.9 | 43.1 | 0.18 ± 0.04 | -0.6 ± 0.1 |
| 12.9 | 15.4 | 0.03 ± 0.03 | -9.1 ± 0.1 |
| 12.9 | 22.2 | 0.07 ± 0.03 | 12.7 ± 0.1 |
| 12.9 | 43.1 | 0.13 ± 0.03 | 2.3 ± 0.1 |
| 15.4 | 22.2 | 0.05 ± 0.03 | 23.5 ± 0.3 |
| 15.4 | 43.1 | 0.09 ± 0.03 | 19.9 ± 0.2 |
| 22.2 | 43.1 | 0.03 ± 0.02 | 33.2 ± 0.4 |

Col. (1) & (2): observed frequency in GHz, Col. (3): magnitude of the core-shift in milliarcseconds, Col. (4): angle of core-shift in degrees. Average angle: $14 \pm 10^\circ$

Table 3. Averaged core-shifts using 43 GHz as the reference frequency for 2200+420, plotted in Fig. 3

| ν (GHz) | Δr (mas) | $\Delta r_{projected}$ (pc) | Fraction of beam (%) |
|----------------|---------------------|--------------------------------|-------------------------|
| 4.6 | 0.46 ± 0.07 | 0.60 ± 0.09 | 17 |
| 5.1 | 0.43 ± 0.07 | 0.56 ± 0.09 | 17 |
| 7.9 | 0.27 ± 0.04 | 0.35 ± 0.05 | 16 |
| 8.9 | 0.21 ± 0.04 | 0.27 ± 0.05 | 14 |
| 12.9 | 0.12 ± 0.03 | 0.16 ± 0.04 | 11 |
| 15.4 | 0.10 ± 0.03 | 0.13 ± 0.04 | 10 |
| 22.2 | 0.04 ± 0.02 | 0.05 ± 0.03 | 5 |

Col. (1): observed frequency in GHz, Col. (2): magnitude of the shift from the 43-GHz core position, Col. (3): projected shift in parsecs (1 mas = 1.3 pc), Col. (4): core-shift as a fraction of the beam-size at the corresponding frequency, in percent.

the de-projected distance of the radio core to the base of the jet, $r_{core}(\nu)$ from eqn. (1), the equipartition magnetic field strength at 1 pc, B_1 from eqn. (5), and finally, using eqn. (6) the magnetic field strength in the radio core. Our results are listed in Table 4.

It's important to note the effect that small changes in the parameter k_r have on our calculated values. We get $0.92 < k_r < 1.06$ from the range of possible values within the error in the fit shown in Fig. 3. There is a strong dependence on the value of $r_{core}(\nu)$ with $3.5 < r_{core}(43 \text{ GHz}) < 0.14 \text{ pc}$, while the magnetic field strength at 1 pc remains relatively insensitive to small variations in k_r with $0.12 < B_1 < 0.14 \text{ pc}$ (using $\Omega_{r\nu}$ at 43 GHz).

Therefore, while there is a rather large uncertainty in r_{core} and hence B_{core} , we consider the calculated value of B_1 to be reliable for the jet parameters listed in Table 1.

Adopting $k_r = 1$, we plot the magnetic field strength in the core as a function of the distance from the base of the jet in Fig. 4. Fitting the line $B(r) = B_1 r^{-1}$ to the data, we find $B_1 = 0.139$ G with a formal error of 0.006 G. By extrapolation, our results predict field strengths of the order of 1 G in the 1 mm core of 2200+420. This is consistent with results for other jets from Savolainen et al. (2008), where he finds magnetic field strengths of order 1 G in the core of 3C 273 by measuring the synchrotron self-absorption turnover frequency (e.g., Marscher 1987) of individual model-fitted components from 5–86 GHz (60–3.5 mm). Importantly, this method does not require the assumption of equipartition to separate the magnetic field strength from the particle number density, but the calculations are very sensitive to the exact values of the turnover frequency and the estimated size of the model-fitted core component at the turnover frequency.

In their simulations of magnetically driven relativistic jets, K07 consider applications of their model to AGN jets and provide a means of estimating the distance from the central engine at which equipartition between the Poynting and matter energy fluxes is established, $R_{eq,BH} \sim 2 \times 10^{16} (M_{BH}/10^8 M_\odot) (0.1/\phi)$ cm, for jets launched from the black hole or from the nuclear accretion disk $R_{eq}(AD) \sim 10^{17} (M_{BH}/10^8 M_\odot) (0.1/\phi)$ cm. In their model, the jet flow is magnetically accelerated up to a distance of $\sim 10R_{eq}$, at which point it reaches the terminal Lorentz factor; hence, observations that probe this region may detect deviations from the jet model of BK79, which assumes a constant jet speed, and possibly infer whether the observed jet has been launched from the black hole or the accretion disk. Using the jet opening angle of 1.9° and a black hole mass of $1.7 \times 10^8 M_\odot$ (Woo & Urry 2002), the equipartition distance for a black-hole-launched jet in 2200+420 is ~ 0.03 pc while $R_{eq} \sim 0.2$ pc for a jet launched from the accretion disk, which according to our results, would be accessible with VLBI observations at frequencies greater than 120 GHz. This is out of the range of current VLBI but could be probed with future sub-mm VLBI arrays (e.g., Doeleman et al. 2009). However, since the terminal Lorentz factor is not reached until $\sim 10R_{eq}$ it's possible that accelerating jet components could be seen in the inner jet at frequencies as low as ~ 15 GHz. Multi-epoch VLBA observations at 43 GHz from Jorstad et al. (2005) have indeed found accelerating jet components for this source which they attribute to a small change in the Lorentz factor along with a substantial change in the direction of the jet flow. The large uncertainty in

Table 4. Derived physical quantities for 2200+420 ($k_r = 1$)

| ν (GHz) | $B_{core}(\nu)$ (G) | $r_{core}(\nu)$ (pc) | B_{1pc} (G) | $\Omega_{r\nu}$ (pc · GHz) |
|----------------|------------------------|-------------------------|------------------|-------------------------------|
| 4.6 | 0.03 ± 0.01 | 5.9 ± 5.0 | 0.16 ± 0.20 | - |
| 5.1 | 0.03 ± 0.01 | 5.4 ± 4.5 | 0.16 ± 0.20 | 3.7 ± 3.1 |
| 7.9 | 0.05 ± 0.01 | 2.5 ± 0.7 | 0.13 ± 0.05 | 2.8 ± 0.7 |
| 8.9 | 0.06 ± 0.01 | 2.5 ± 0.6 | 0.14 ± 0.05 | 3.0 ± 0.8 |
| 12.9 | 0.08 ± 0.01 | 1.9 ± 0.4 | 0.15 ± 0.05 | 3.3 ± 0.7 |
| 15.4 | 0.09 ± 0.01 | 1.6 ± 0.3 | 0.15 ± 0.04 | 3.4 ± 0.6 |
| 22.2 | 0.14 ± 0.02 | 1.1 ± 0.3 | 0.14 ± 0.06 | 3.1 ± 0.9 |
| 43.1 | 0.27 ± 0.02 | 0.5 ± 0.1 | 0.13 ± 0.03 | 2.8 ± 0.4 |

Col. (1): observed frequency in GHz, Col. (2): radio core magnetic field strength in Gauss, Col. (3): de-projected distance of the radio core to the base of the jet in parsecs, Col. (4): magnetic field strength at 1 pc, Col. (5): average core-position offset measure, in units of pc · GHz, for shifts with ν_2 in Table 2 equal to ν in Col. (1) above. Note: Physical parameters at 4.6 GHz calculated with 5.1 GHz core-position offset measure.

r_{core} should be kept in mind though, as $r_{core}(43 \text{ GHz})$ may extend as far as 3.5 pc from the base of the jet.

Using the divergence theorem, we can also estimate the initial magnetic field strength at the jet launching distance by assuming the energy extracted per time is equal to the Poynting flux times the area (N. Vlahakis, private communication), which gives $B_0 \sim 1.5 \times 10^{-5} L^{1/2} r^{-1}$. For example, with $L \sim 10^{46} \text{ erg s}^{-1}$ and $M_{BH} \sim 10^8 M_{\odot}$, we get $B_{0,AD} \sim 10^4 \text{ G}$ at an inner accretion disk distance of $10r_g$ and $B_0(BH) \sim 10^5 \text{ G}$ at a black hole jet-launching distance of r_g , as quoted in K07.

Using eqn. (23) from BK79, we can find an estimate for the total power carried by the relativistic electrons and magnetic field in the jet, $L_{total} \sim 2.5 \times 10^{48} \Gamma^2 \beta \phi^2 B_1^2 \text{ erg s}^{-1}$, where β is the speed of the jet in units of c . From our best-fit value of $B_1 \sim 0.14 \text{ G}$, we get $L_{total} \sim (2.6 \pm 0.2) \times 10^{45} \text{ erg s}^{-1}$. Hence, for 2200+420, we expect $B_0(AD) \sim 3 \times 10^3 \text{ G}$ and $B_0(BH) \sim 3 \times 10^4 \text{ G}$. In Fig. 5, we extend our plot of B vs. r to include the calculated values of the initial magnetic field strength at the corresponding jet launching distances. Extrapolating $0.14r^{-1}$ all the way down to $1r_g$, we find $B \sim 1.7 \times 10^4 \text{ G}$, in good agreement with the estimated magnetic strengths at the nominal jet launching distances.

3.2 2007+777

In Fig. 6 we show the spectral index distribution of 2007+777 from 4.6–43 GHz. For this source we find a flat to inverted spectrum in the core region, falling off to a steep optically thin spectrum further downstream in the jet. The slices for the 4.6–7.9 GHz and 8.9–12.9 GHz maps (Fig.6a, b) show optically thick regions at the edge of the jet $\sim 8 \text{ mas}$ from the core; however, these are possibly spurious features due to edge effects when combining the

two maps. We only show the spectral index map from 15.4–43 GHz due to loss of flux in the 22-GHz map.

All measured core-shifts for 2007+777 are listed in Table 5. The average direction of the measured shift is $89 \pm 13^\circ$, which is consistent with the parsec scale jet direction of $\sim -90^\circ$. The y-intercept of the best-fit line to the data (Fig. 7) is -0.001 ± 0.004 , indicating that the compact jet region from 4.6–43 GHz is close to equipartition. Due to a failure to find shift measurements that produced reasonable spectral index maps combining the higher frequencies with the 7.9 and 8.9 GHz images, we do not have as many measurements as in the previous case of 2200+420. In order to make the spectral index map between 8.9 and 12.9 GHz, we use in Fig. 6 the characteristic position-offset measure of $5.2 \pm 0.3 \text{ pc} \cdot \text{GHz}$ from the best-fit line to the measured data in Fig. 7 to estimate the required shift. This produces a spectral index map consistent with those generated at lower and higher frequencies (Fig. 6). In order to find an estimate for the parameter k_r , we use over-lapping shifts to plot 7.9–43 GHz and 8.9–43 GHz values (e.g., $(4.6\text{--}15.4 \text{ GHz}) - (4.6\text{--}7.9 \text{ GHz}) + (15.4\text{--}43 \text{ GHz})$). Hence, we find $k_r = 0.97 \pm 0.06$ (Fig. 8) for this source (see Table 6 for listed values). Without the 7.9–43 GHz and 8.9–43 GHz points, we get $k_r = 0.99 \pm 0.05$.

Gabuzda et al. (1994) find $\beta_{\text{app}} = 2.9$ for 2007+777, where β_{app} is the apparent velocity of the jet in units of the speed of light, based on three observations between 1980 and 1989. However, from much more densely sampled multi-epoch monitoring from 1994–2002 at 15 GHz, Kellermann et al. (2004) do not detect any outward motion from the jet of 2007+777. Hovatta et al. (2009) derive a Doppler factor (δ) of 7.9 using variability arguments from single dish monitoring indicating that this jet does have a relativistic flow. To estimate the magnetic field strength in this source, we require estimates for the bulk Lorentz factor (Γ) and the viewing angle (θ). Due to the uncertainty in the jet speed measurements, we assume $\beta_{\text{app}} \sim \delta$ and from this we find the minimum Lorentz factor of the flow from $\Gamma_{\text{min}} = (1 + \beta_{\text{app}}^2)^{1/2}$. To estimate the viewing angle we use $\theta = \sin^{-1}(1/\Gamma_{\text{min}})$; while this is unlikely to be true for any one source, it is a good approximation in a statistical sense (see Cohen et al. 2007). We find a jet opening angle of 1.0° by estimating the projected half opening angle using the ratio between the apparent transverse size and longitudinal distance of the jet components within 1 mas from the core (i.e., we assume a conical jet with a constant opening angle within this region, see also Jorstad et al. (2005)).

Due to the absence of direct jet speed measurements, the following magnetic field values can only be considered as rough estimates. Using the same procedure as described in the

Table 5. All measured core-shifts for 2007+777, plotted in Fig. 7

| ν_1 (GHz) | ν_2 (GHz) | Δr (mas) | Angle ($^\circ$) |
|------------------|------------------|---------------------|-----------------------|
| 4.6 | 5.1 | 0.02 ± 0.02 | 91 ± 1 |
| 4.6 | 7.9 | 0.10 ± 0.02 | 89 ± 1 |
| 4.6 | 8.9 | 0.12 ± 0.02 | 89 ± 1 |
| 4.6 | 12.9 | 0.15 ± 0.02 | 79 ± 1 |
| 4.6 | 15.4 | 0.17 ± 0.02 | 87 ± 1 |
| 5.1 | 7.9 | 0.08 ± 0.02 | 97 ± 1 |
| 5.1 | 8.9 | 0.10 ± 0.02 | 88 ± 1 |
| 5.1 | 12.9 | 0.12 ± 0.02 | 82 ± 1 |
| 5.1 | 15.4 | 0.13 ± 0.02 | 92 ± 1 |
| 7.9 | 8.9 | 0.02 ± 0.01 | 91.2 ± 0.8 |
| 12.9 | 15.4 | 0.016 ± 0.007 | 117.1 ± 0.3 |
| 12.9 | 22.2 | 0.030 ± 0.007 | 104.1 ± 0.4 |
| 12.9 | 43.1 | 0.055 ± 0.007 | 84.4 ± 0.4 |
| 15.4 | 22.2 | 0.018 ± 0.007 | 54.8 ± 0.3 |
| 15.4 | 43.1 | 0.045 ± 0.007 | 86.7 ± 0.4 |
| 22.2 | 43.1 | 0.022 ± 0.006 | 83.5 ± 0.3 |

Col. (1) & (2): observed frequency in GHz, Col. (3): magnitude of the core-shift in milliarcseconds, Col. (4): angle of core-shift in degrees. Average angle: $89 \pm 13^\circ$

case of 2200+420, the calculated B_{core} , r_{core} and B_1 are presented in Table 7 using the equipartition value of $k_r = 1$ and a jet spectral index of -0.5 consistent with the spectral index maps (Fig. 6). Considering a range of values for k_r , from the fit to the data shown in Fig. 8, of $0.91 < k_r < 1.03$, we get $8.7 < r_{core}(43 \text{ GHz}) < 0.5 \text{ pc}$ and $0.23 < B_1 < 0.27 \text{ pc}$ (using $\Omega_{r\nu}$ at 43 GHz).

We plot B_{core} versus r_{core} , for $k_r = 1$, in Fig. 9 and find $B_1 = 0.257 \pm 0.007 \text{ G}$. Extending this line to the launching region of the jet (Fig. 10), we find that it reaches $\sim 1.3 \times 10^3 \text{ G}$ at an accretion disk distance of $10r_g$ and $\sim 1.3 \times 10^4 \text{ G}$ at r_g , using a black hole mass of $4.0 \times 10^8 M_\odot$ (Wu et al. 2009). We calculate the total jet power using $B_1 \simeq 0.26 \text{ G}$ and with the jet parameters listed in Table 1 to find $L_{total} \sim (3.2 \pm 0.2) \times 10^{45} \text{ erg s}^{-1}$. Using L_{total} , we estimate the magnetic field strength of $B_0 \sim 1.4 \times 10^3 \text{ G}$ at the jet launching distance of $10r_g$, which is in excellent agreement with our extrapolated magnetic field strength results (Fig. 10).

The estimated equipartition radius for an accretion-disk-launched jet of $\sim 0.7 \text{ pc}$ is just outside the range of 43-GHz VLBI, which probes distances of $\sim 0.9 \text{ pc}$ from the central engine (Fig. 10). However, this source should be a good candidate for the possible detection of accelerating jet components from multi-epoch monitoring at 43 GHz, even though the 43-GHz core may extend as far as $\sim 9 \text{ pc}$ from the base of the jet, since the jet flow is not expected to reach its terminal Lorentz factor until $\sim 1 \text{ pc}$ for a black-hole-launched jet and $\sim 7 \text{ pc}$ for an accretion-disk-launched jet.

Table 6. Averaged core-shifts using 43 GHz as the reference frequency for 2007+777, plotted in Fig. 8

| ν (GHz) | Δr (mas) | $\Delta r_{projected}$ (pc) | Fraction of beam (%) |
|----------------|---------------------|--------------------------------|-------------------------|
| 4.6 | 0.21 ± 0.02 | 1.0 ± 0.1 | 9 |
| 5.1 | 0.17 ± 0.02 | 0.8 ± 0.1 | 8 |
| 7.9 | 0.10 ± 0.02 | 0.5 ± 0.1 | 7 |
| 8.9 | 0.08 ± 0.02 | 0.4 ± 0.1 | 6 |
| 12.9 | 0.056 ± 0.007 | 0.27 ± 0.03 | 6 |
| 15.4 | 0.042 ± 0.007 | 0.20 ± 0.03 | 6 |
| 22.2 | 0.025 ± 0.006 | 0.12 ± 0.03 | 5 |

Col. (1): observed frequency in GHz, Col. (2): magnitude of the shift from the 43-GHz core position, Col. (3): projected shift in parsecs (1 mas = 4.8 pc), Col. (4): core-shift as a fraction of the beam-size at the corresponding frequency, in percent.

Table 7. Derived physical quantities for 2007+777 ($k_r = 1$)

| ν (GHz) | $B_{core}(\nu)$ (G) | $r_{core}(\nu)$ (pc) | B_{1pc} (G) | $\Omega_{r\nu}$ (pc · GHz) |
|----------------|------------------------|-------------------------|------------------|-------------------------------|
| 4.6 | 0.030 ± 0.010 | 8.7 ± 4.9 | 0.26 ± 0.22 | - |
| 5.1 | 0.034 ± 0.010 | 7.8 ± 4.4 | 0.26 ± 0.22 | 5.0 ± 2.8 |
| 7.9 | 0.051 ± 0.003 | 5.5 ± 0.7 | 0.28 ± 0.05 | 5.5 ± 0.7 |
| 8.9 | 0.056 ± 0.003 | 5.4 ± 0.5 | 0.30 ± 0.05 | 6.0 ± 0.6 |
| 12.9 | 0.085 ± 0.005 | 3.1 ± 0.3 | 0.26 ± 0.04 | 5.0 ± 0.5 |
| 15.4 | 0.099 ± 0.005 | 2.8 ± 0.3 | 0.28 ± 0.04 | 5.5 ± 0.5 |
| 22.2 | 0.15 ± 0.01 | 1.6 ± 0.3 | 0.24 ± 0.06 | 4.4 ± 0.7 |
| 43.1 | 0.28 ± 0.03 | 0.9 ± 0.2 | 0.26 ± 0.07 | 5.0 ± 0.9 |

Col. (1): observed frequency in GHz, Col. (2): radio core magnetic field strength in Gauss, Col. (3): de-projected distance of the radio core to the base of the jet in parsecs, Col. (4): magnetic field strength at 1 pc, Col. (5): average core-position offset measure, in units of $10^9 \text{ pc} \cdot \text{GHz}$, for shifts with ν_2 in Table 5 equal to ν in Col. (1) above. Note: Physical parameters at 4.6 GHz calculated with 5.1 GHz core-position offset measure.

3.3 1418+546

Fig. 11 shows the spectral index distribution from 4.6–43 GHz for the source 1418+546. We find an inverted core spectrum between the lower frequency pairs (Fig. 11a, b, c) with a flat spectrum core region between 22 and 43 GHz (Fig. 11d). In the 4.6–7.9 GHz map (Fig. 11a) the jet spectral index is ~ -0.2 , while at higher frequencies it becomes steeper with a typical value of -0.5 (Fig. 11b, c).

The best fit line to the measured shifts listed in Table 8 gives a y-intercept of 0.003 ± 0.004 assuming $k_r = 1$ and the slope provides a characteristic $\Omega_{r\nu} = 3.9 \pm 0.2 \text{ pc} \cdot \text{GHz}$ (Fig. 12). The average position angle of the shift is $-52 \pm 13^\circ$, consistent within the errors with the inner jet direction at 43 GHz of $\sim 137^\circ$. Again averaging the measured shifts and using 43 GHz as the reference frequency (Table 9), we find $k_r = 1.08 \pm 0.11$ between 4.6 and 43 GHz (Fig. 13). The equipartition value $k_r = 1$ and $\alpha_j = -0.5$ are used to calculate the physical parameters listed in Table 10. We estimate a jet opening angle of 1.9° from the size of the jet components within 1 mas from the core. We use a Doppler factor of 5.1 from Hovatta et al. (2009) and $\beta_{app} = 4.3$ from Pushkarev & Gabuzda (1999) to find estimates

Table 8. All measured core-shifts for 1418+546, plotted in Fig. 12

| ν_1 (GHz) | ν_2 (GHz) | Δr (mas) | Angle ($^\circ$) |
|------------------|------------------|---------------------|-----------------------|
| 4.6 | 5.1 | 0.03 ± 0.02 | -38.2 ± 0.9 |
| 4.6 | 7.9 | 0.14 ± 0.02 | -49.6 ± 0.7 |
| 4.6 | 8.9 | 0.15 ± 0.02 | -44.0 ± 0.6 |
| 4.6 | 12.9 | 0.20 ± 0.02 | -51.7 ± 0.7 |
| 4.6 | 15.4 | 0.23 ± 0.02 | -60.3 ± 0.5 |
| 5.1 | 7.9 | 0.11 ± 0.02 | -41.5 ± 0.8 |
| 5.1 | 8.9 | 0.13 ± 0.02 | -35.8 ± 0.6 |
| 5.1 | 12.9 | 0.17 ± 0.02 | -46.8 ± 0.4 |
| 5.1 | 15.4 | 0.21 ± 0.02 | -54.0 ± 0.5 |
| 7.9 | 8.9 | 0.02 ± 0.02 | -24.3 ± 0.7 |
| 7.9 | 12.9 | 0.07 ± 0.02 | -53.2 ± 0.7 |
| 7.9 | 15.4 | 0.11 ± 0.02 | -57.4 ± 0.2 |
| 8.9 | 12.9 | 0.06 ± 0.02 | -58.4 ± 0.9 |
| 8.9 | 15.4 | 0.09 ± 0.02 | -68.3 ± 0.7 |
| 12.9 | 15.4 | 0.021 ± 0.007 | -82.4 ± 0.3 |
| 15.4 | 22.2 | 0.030 ± 0.007 | -62.7 ± 0.3 |
| 22.2 | 43.1 | 0.036 ± 0.005 | -56.2 ± 0.2 |

Col. (1) & (2): observed frequency in GHz, Col. (3): magnitude of the core-shift in milliarcseconds, Col. (4): angle of core-shift in degrees. Average angle: $-52 \pm 13^\circ$

of the bulk Lorentz factor of 4.5 using $\Gamma = (\beta_{\text{app}}^2 + \delta^2 + 1)/(2\delta)$ and the jet viewing angle of 11.2° using $\theta = \tan^{-1}((2\beta_{\text{app}})/(\beta_{\text{app}}^2 + \delta^2 - 1))$ (e.g., Hovatta et al. 2009).

We find $B_1 = 0.178 \pm 0.006$ G from our plot of B_{core} versus r_{core} (Fig. 14). Extrapolating this line, we find $B \sim 680$ G at an accretion disk distance of $10r_g$, using the black hole mass estimate of $10^{8.74}$ from Wu et al. (2009). Using the calculated total luminosity of $(1.7 \pm 0.1) \times 10^{45}$ erg s $^{-1}$, we expect $B_0 \sim 750$ G at $10r_g$ from the divergence theorem (Fig. 15).

For $0.97 < k_r < 1.19$, we get $1.1 < r_{\text{core}}(43 \text{ GHz}) < 0.01$ pc and $0.18 < B_1 < 0.21$ pc (using $\Omega_{r\nu}$ at 43 GHz). An interesting feature of this source is that the estimated equipartition radius for an accretion-disk-launched jet ($R_{eq} \sim 0.5$ pc) is within the range of VLBI observations at 43 GHz assuming $k_r \sim 1$. Multi-epoch VLBI monitoring of this jet at 43 GHz should provide evidence for the extended acceleration predicted from the magnetically driven jet model of K07 since the jet flow is not expected to reach its terminal Lorentz factor until a distance of ~ 1 pc for a black-hole-launched jet and ~ 5 pc for an accretion-disk-launched jet.

3.4 0954+658

In Fig. 16 we show the spectral index maps for 0954+658 from 4.6–43 GHz. We observe a strongly inverted spectrum from 4.6–22 GHz in the core region (Fig. 16a, b, c), which then flattens considerably at the highest frequencies (Fig. 16d). We note the spectral index gradient across the jet in the 4.6–7.9 GHz image, which is discussed in O’Sullivan & Gabuzda

Table 9. Averaged core-shifts using 43 GHz as reference frequency for 1418+546, plotted in Fig. 13

| ν (GHz) | Δr (mas) | $\Delta r_{projected}$ (pc) | Fraction of beam (%) |
|----------------|---------------------|--------------------------------|-------------------------|
| 4.6 | 0.29 ± 0.02 | 0.75 ± 0.05 | 10 |
| 5.1 | 0.27 ± 0.02 | 0.70 ± 0.05 | 10 |
| 7.9 | 0.16 ± 0.02 | 0.42 ± 0.05 | 9 |
| 8.9 | 0.13 ± 0.02 | 0.34 ± 0.05 | 9 |
| 12.9 | 0.085 ± 0.007 | 0.22 ± 0.02 | 8 |
| 15.4 | 0.066 ± 0.007 | 0.17 ± 0.02 | 8 |
| 22.2 | 0.036 ± 0.005 | 0.09 ± 0.01 | 6 |

Col. (1): observed frequency in GHz, Col. (2): magnitude of the shift from the 43-GHz core position, Col. (3): projected shift in parsecs (1 mas = 2.6 pc), Col. (4): core-shift as a fraction of the beam-size at the corresponding frequency, in percent.

Table 10. Derived physical quantities for 1418+546 ($k_r = 1$)

| ν (GHz) | $B_{core}(\nu)$ (G) | $r_{core}(\nu)$ (pc) | B_{1pc} (G) | $\Omega_{r\nu}$ (pc · GHz) |
|----------------|------------------------|-------------------------|------------------|-------------------------------|
| 4.6 | 0.040 ± 0.011 | 4.1 ± 2.3 | 0.16 ± 0.14 | - |
| 5.1 | 0.044 ± 0.012 | 3.7 ± 2.1 | 0.16 ± 0.14 | 3.7 ± 2.0 |
| 7.9 | 0.067 ± 0.004 | 2.7 ± 0.3 | 0.18 ± 0.03 | 4.1 ± 0.4 |
| 8.9 | 0.076 ± 0.004 | 2.2 ± 0.2 | 0.17 ± 0.02 | 3.8 ± 0.4 |
| 12.9 | 0.11 ± 0.01 | 1.6 ± 0.3 | 0.17 ± 0.06 | 3.9 ± 0.8 |
| 15.4 | 0.13 ± 0.01 | 1.5 ± 0.2 | 0.19 ± 0.03 | 4.4 ± 0.5 |
| 22.2 | 0.19 ± 0.02 | 0.9 ± 0.2 | 0.17 ± 0.04 | 4.0 ± 0.7 |
| 43.1 | 0.36 ± 0.02 | 0.52 ± 0.05 | 0.19 ± 0.03 | 4.3 ± 0.4 |

Col. (1): observed frequency in GHz, Col. (2): radio core magnetic field strength in Gauss, Col. (3): de-projected distance of the radio core to the base of the jet in parsecs, Col. (4): magnetic field strength at 1 pc, Col. (5): average core-position offset measure, in units of 10^9 pc · GHz, for shifts with ν_2 in Table 8 equal to ν in Col. (1) above. Note: Physical parameters at 4.6 GHz calculated with 5.1 GHz core-position offset measure.

(2009). The region of inverted spectrum at ~ 3 mas from the core in the 8.9–12.9 GHz map (Fig. 16b) may also be connected with the change in the jet direction in the plane of the sky. The extended emission in this source falls off sharply with increasing frequency, which is why we could not obtain core-shift measurements at frequencies higher than 8.9 GHz.

We obtained two reliable core-shift measurements for the jet of 0954+658, with the angle of the shifts ($\sim 127^\circ$) consistent with the inner jet direction at 43 GHz of $\sim -59^\circ$ (Table 11). In this case, we assume a value of $k_r = 1$ from 4.6–43 GHz due to our lack of measurements, and calculate the shifts with which to align our images from this. The spectral index maps in Fig. 16 indicate that this is a reasonable assumption between 4.6 and 43 GHz, providing a flat to inverted core spectrum with a steep spectrum jet as expected.

In order to estimate the magnetic field strength for this source, we use a Doppler factor of 6.2 from Hovatta et al. (2009) and $\beta_{app} = 6.2$ from Gabuzda et al. (1994) to find $\Gamma = 6.3$ and $\theta = 9.3^\circ$. We get $\phi = 2.2^\circ$ from the size of jet components within 1 mas of the core. We use a jet spectral index of -0.6 throughout the calculations due to the steep fall-off in the jet spectral index. In this case, to calculate the magnetic field strength we need to assume a value for the lower cut-off in the electron energy distribution since $B_1 \propto \gamma_{min}^{-0.05}$. Using

Table 11. Measured core-shifts for 0954+658

| ν_1 (GHz) | ν_2 (GHz) | Δr (mas) | Angle ($^\circ$) | fraction of beam (%) |
|------------------|------------------|---------------------|-----------------------|-------------------------|
| 4.6 | 7.9 | 0.16 ± 0.02 | 126.8 ± 0.6 | 6 |
| 4.6 | 8.9 | 0.18 ± 0.02 | 127.3 ± 0.6 | 7 |

Col. (1) & (2): observed frequency in GHz, Col. (3): magnitude of the core-shift in milliarcseconds, Col. (4): angle of core-shift in degrees. Col. (5): core-shift as a fraction of the 4.6-GHz beam-size, in percent.

Table 12. Derived physical quantities for 0954+658

| ν (GHz) | $B_{core}(\nu)$ (G) | $r_{core}(\nu)$ (pc) | B_{1pc} (G) | $\Omega_{r\nu}$ (pc · GHz) |
|----------------|------------------------|-------------------------|------------------|-------------------------------|
| 7.9 | 0.038 ± 0.002 | 7.0 ± 0.6 | 0.27 ± 0.03 | 8.9 ± 0.7 |
| 8.9 | 0.044 ± 0.002 | 6.0 ± 0.4 | 0.27 ± 0.03 | 8.7 ± 0.6 |

Col. (1): observed frequency in GHz, Col. (2): radio core magnetic field strength in Gauss, Col. (3): de-projected distance of the radio core to the base of the jet in parsecs, Col. (4): magnetic field strength at 1 pc, Col. (5): average core-position offset measure, in units of $10^9 \text{pc} \cdot \text{GHz}$, for shifts with ν_2 in Table 11 equal to ν in Col. (1) above. Note: magnetic field strengths calculated for $\gamma_{\min} = 100$

$\Omega_{r\nu} = 8.8 \pm 0.7 \text{ pc} \cdot \text{GHz}$, we get $B_1 = 0.27 \pm 0.03 \text{ G}$ with $\gamma_{\min} = 100$ while if γ_{\min} extends all the way down to 1, we get $B_1 = 0.34 \pm 0.05 \text{ G}$. Our estimates of the physical parameters for this source are shown in Table 12 assuming $\gamma_{\min} = 100$ and $\alpha = -0.6$.

Extrapolating these measurements, we estimate a magnetic field strength in the 43 GHz radio core of $B_{core} \sim 0.21 \text{ G}$ at a distance of $r_{core} \sim 1.3 \text{ pc}$. Using a black hole mass of $10^{8.37} M_\odot$ (Wu et al. 2009), we find $R_{\text{eq,AD}} \sim 0.2 \text{ pc}$ and $R_{\text{eq}}(BH) \sim 0.02 \text{ pc}$. From the calculated total luminosity of $(1.1 \pm 0.2) \times 10^{46} \text{ erg s}^{-1}$, we expect $B_0 \sim 4 \times 10^3$ from the divergence theorem. Using $B(r) = 0.27r^{-1}$, we find $B \sim 2 \times 10^3 \text{ G}$ at $10r_g$.

3.5 1156+295 and 1749+096

For these two sources, we were unable to obtain core-shift measurements due to the weak nature of the jet emission. Hence, in this case we cannot be sure if the core corresponds to a stationary feature or the $\tau = 1$ surface. To produce the spectral index maps (Figs. 17, 18), we aligned the images by their model-fitted core positions. This produced uniform flat spectra in the core regions (e.g., the slice along the 4.6–7.9 GHz spectral index map for 1156+295, Fig. 17a). We can see that the core spectrum of 1156+295, is strongly inverted ($\alpha_{7.9\text{GHz}}^{4.6\text{GHz}} \sim 1.3$) at low frequencies and then flattens considerably at the higher frequencies with $\alpha_{43\text{GHz}}^{22\text{GHz}} \sim -0.05$ (Fig. 17). The core spectrum of 1749+096 (Fig. 18) displays similar properties, with $\alpha_{7.9\text{GHz}}^{4.6\text{GHz}} \sim 1.0$ and becomes flat at the highest frequencies with $\alpha_{43\text{GHz}}^{22\text{GHz}} \sim 0.01$.

4 DISCUSSION

In principle, the position of the vertex of the cone should provide a good estimate for the location of the central supermassive black hole powering the jet given that the distance to the radio core is likely to be much greater than the distance to the jet injection point or jet “nozzle”. However, the exact position is uncertain due to the strong dependence of r_{core} on small deviations in the value of k_r . In the case of 2200+420, the base of the jet can have a projected separation of up to $r_{proj,max} \sim 0.4$ mas (~ 0.5 pc for $k_r = 0.92$) from the 43-GHz core. For 2007+777 and 1418+546, we find $r_{proj,max} \sim 0.2$ mas ($k_r = 0.91$) and ~ 0.1 mas ($k_r = 0.97$), respectively, from their 43-GHz cores. Only the errors in the core-shift measurements are taken into account for our magnetic field strength calculations, hence, the results may be subject to systematic errors if one or more of the jet parameters (ϕ , θ , Γ , δ) are inaccurate. Of course all values presented here should be considered in the context of the assumption that the jet speed measurements accurately reflect the bulk flow speed of the jet and not some pattern speed.

The main result from our core-shift measurements is that we find equipartition between the particle and magnetic field energy densities to be an accurate assumption for the radio core of the observed sources from 4.6–43 GHz. Conservation of particle number in a freely expanding conical jet requires $N \propto r^{-2}$, which then implies $B \propto r^{-1}$ from equipartition. Furthermore, we expect the longitudinal magnetic field strength to fall-off as r^{-2} and the transverse component to fall-off as r^{-1} (Begelman, Blandford & Rees 1984; Hutter & Mufson 1986) so that over most of the length of the jet the transverse component will dominate and the overall magnetic field strength will scale as r^{-1} . This is also seen in models of magnetically dominated relativistic jets (Vlahakis & Königl 2004) where, after the poloidal component of the magnetic field initially dominates, the toroidal component dominates at large distances and follows an approximate r^{-1} fall-off in field strength. Our results are well described by $B \propto r^{-1}$, and by extrapolating back to the jet launching region, we get magnetic field strengths consistent with those required by models of magnetically launched jets to produce the observed jet luminosities.

The implication of finding $N \propto r^{-2}$ consistent with our results is that, in the radio core from 4.6–43 GHz, continuous re-acceleration of the emitting particles is required to offset both the radiation and adiabatic expansion losses in this region. This could be achieved

Table 13. Particle number density estimates at 1 pc for each source ($k_r = 1$).

| Source | $N_1(\gamma_{\min} = 1)$ (cm^{-3}) | $N_1(\gamma_{\min} = 100)$ (cm^{-3}) |
|----------|--|--|
| 0954+658 | 1061 | 6.8 |
| 1156+295 | – | – |
| 1418+546 | 223 | 2.2 |
| 1749+096 | – | – |
| 2007+777 | 354 | 3.5 |
| 2200+420 | 103 | 1.0 |

Col. (1): IAU source name, Col. (2): particle number density at 1 pc in cm^{-3} for a pair plasma with $\gamma_{\min} = 1$, Col. (3): particle number density at 1 pc in cm^{-3} for a normal plasma with $\gamma_{\min} = 100$.

through numerous shocks (Marscher & Gear 1985), magnetic reconnection (Zenitani & Hoshino 2008) and/or turbulence from Kelvin-Helmholtz or current-driven instabilities.

In order to decouple the magnetic field strength from the particle number density, we used the equipartition condition of equation 3. We can now put the calculated B_1 back into the equation to get an estimate for the particle number density at 1 pc. However, we also need to assume a value for the lower cut-off of the electron energy distribution (γ_{\min}). For a jet dominated by a normal (electron-proton) plasma, the energy distribution must have a cut-off of $\gamma_{\min} \leq 100$ (Ghisellini et al. 1992; Wardle et al. 1998), while for an electron-positron jet γ_{\min} can extend all the way down to 1 (Reynolds et al. 1996; Hirovani 2005). In Table 13, we list the particle number density in the jet at 1 parsec (N_1) for γ_{\min} equal to 1 and to 100.

Extended jet acceleration regions, most likely caused by MHD and/or hydrodynamical forces, have been detected in several AGN jets with the high resolution of VLBI (e.g., Jorstad et al. 2005). From the model of K07, we can calculate the distance at which the jet approaches its terminal Lorentz factor. From this, we find that 2200+420, 2007+777 and 1418+546 would be interesting candidates for the detection of extended jet acceleration from VLBI monitoring, since the terminal Lorentz factor distance for accretion-disk-launched jets for these sources extends beyond the distance of the 43-GHz VLBI core from the base of the jet. Jorstad et al. (2005) have already detected accelerating components from 43 GHz VLBA monitoring of 2200+420 providing more weight to the estimates presented in this paper.

Finally, we stress the importance of continued VLBI jet monitoring to obtain estimates of jet speeds, viewing angles and Doppler factors to enable magnetic field strength calculations for a much larger sample of AGN.

5 CONCLUSIONS

From our measurements of the frequency dependent position of the VLBI radio core, we find that:

1. The jets of 2200+420, 2007+777 and 1418+546 from 4.6–43 GHz are well described by the conical jet model of BK79 with $r_{\text{core}}(\nu) \propto \nu^{-1/k_r}$. Furthermore, power-law fits to the data strongly support the equipartition value of $k_r = 1$ in this region.

2. Our spectral index maps are also consistent with the BK79 jet model of an optically thick, unresolved jet base with all maps displaying a flat or inverted spectrum in the core region, turning over to an optically-thin steep-spectrum region further downstream in the jet.

3. We calculate equipartition magnetic field strengths with typical values from 10's to 100's of mG in the 4.6–43 GHz radio cores. Extrapolation of our results, following an r^{-1} power law, to the accretion disk and black hole jet-launching distances gives magnetic field strengths in general agreement with those expected from theoretical models of magnetically powered jets.

ACKNOWLEDGEMENTS

Funding for this research was provided by the Irish Research Council for Science, Engineering and Technology. The authors would like to thank Nektarios Vlahakis, Serguei Komissarov, Andrei Lobanov, Heino Falcke and Yuri Kovalev for their help as well as the anonymous referee for valuable comments that substantially improved this paper. The VLBA is a facility of the NRAO, operated by Associated Universities Inc. under cooperative agreement with the NSF. This research has made use of NASA's Astrophysics Data System Service.

REFERENCES

- Begelman M. C., Blandford R. D., Rees M. J., 1984, *Reviews of Modern Physics*, 56, 255
 Blandford R. D., Königl A., 1979, *ApJ*, 232, 34
 Blandford R. D., Rees M. J., 1974, *MNRAS*, 169, 395
 Bogovalov S., Tsinganos K., 2005, *MNRAS*, 357, 918
 Cawthorne T. V., 2006, *MNRAS*, 367, 851
 Cohen M. H., Lister M. L., Homan D. C., Kadler M., Kellermann K. I., Kovalev Y. Y., Vermeulen R. C., 2007, *The Astrophysical Journal*, 658, 232

- Croke S., Gabuzda D. C., 2008, *MNRAS*, 386, 619
- Daly R. A., Marscher A. P., 1988, *ApJ*, 334, 539
- Doeleman S. S., Fish V. L., Broderick A. E., Loeb A., Rogers A. E. E., 2009, *ApJ*, 695, 59
- Gabuzda D. C., Mullan C. M., Cawthorne T. V., Wardle J. F. C., Roberts D. H., 1994, *MNRAS*, 435, 140
- Ghisellini G., Celotti A., George I. M., Fabian A. C., 1992, *MNRAS*, 258, 776
- Hirota K., 2005, *ApJ*, 619, 73
- Hovatta T., Valtaoja E., Tornikoski M., Lähteenmäki A., 2009, *A&A*, 494, 527
- Hutter D. J., Mufson S. L., 1986, *ApJ*, 301, 50
- Jorstad S. G., Marscher A. P., Lister M. L., Stirling A. M., Cawthorne T. V., Gear W. K., Gómez J. L., Stevens J. A., Smith P. S., Forster J. R., Robson E. I., 2005, *AJ*, 130, 1418
- Kellermann K. I., Lister M. L., Homan D. C., Vermeulen R. C., Cohen M. H., Ros E., Kadler M., Zensus J. A., Kovalev Y. Y., 2004, *The Astrophysical Journal*, 609, 539
- Komissarov S. S., Barkov M. V., Vlahakis N., Königl A., 2007, *MNRAS*, 380, 51
- Königl A., 1981, *ApJ*, 243, 700
- Königl A., 2007, in *Revista Mexicana de Astronomia y Astrofisica Vol. 27 of Revista Mexicana de Astronomia y Astrofisica Conference Series, MHD Driving of Relativistic Jets.* pp 91–101
- Kovalev Y., Lobanov A., Pushkarev A., Zensus J., 2008, *A&A*, 483, 759
- Lobanov A., 2006, *Proceedings of the 8th European VLBI Network Symposium. September 26-29*, <http://pos.sissa.it>, p.3
- Lobanov A. P., 1998a, *A&A*, 330, 79
- Lobanov A. P., 1998b, *A&A*, 132, 261
- Marcaide J. M., Shapiro I. I., 1984, *ApJ*, 276, 56
- Marscher A. P., 1987, in Zensus J. A., Pearson T. J., eds, *Superluminal Radio Sources.* Vol. 280. Cambridge Univ. Press
- Marscher A. P., 2009, in Hagiwara Y., Fomalont E., Tsuboi M., Murata Y., eds, *Approaching Micro-Arcsecond Resolution with VSOP-2: Astrophysics and Technology.* Vol. 402. ASP Conf. Ser., San Francisco., p. 194
- Marscher A. P., Gear W. K., 1985, *ApJ*, 298, 114
- Meier D. L., 2009, in Hagiwara Y., Fomalont E., Tsuboi M., Murata Y., eds, *Approaching Micro-Arcsecond Resolution with VSOP-2: Astrophysics and Technology.* Vol. 402. ASP Conf. Ser., San Francisco., p. 342

- Mutel R. L., Phillips R. B., Su B., Bucciferro R. R., 1990, *ApJ*, 351, 81
- O’Sullivan S. P., Gabuzda D. C., 2008, Proceedings of the 9th EVN Symposium, <http://pos.sissa.it>, p.16
- O’Sullivan S. P., Gabuzda D. C., 2009, *MNRAS*, 393, 429
- Pushkarev A. B., Gabuzda D. C., 1999, in L. O. Takalo & A. Sillanpää ed., *BL Lac Phenomenon Vol. 159 of Astronomical Society of the Pacific Conference Series, Second-Epoch VLBI Polarization Observations of Two 1 Jy BL Lac Objects.* p. 458
- Reynolds C. S., Fabian A. C., Celotti A., Rees M. J., 1996, *MNRAS*, 283, 873
- Rybicki G. B., Lightman A. P., 1979, New York, Wiley-Interscience
- Savolainen T., Wiik K., Valtaoja E., Tornikoski M., 2008, Proceedings of the 9th EVN Symposium, <http://pos.sissa.it>, p.9
- Shepherd M. C., 1997, in G. Hunt & H. Payne ed., *Astronomical Data Analysis Software and Systems VI Vol. 125 of Astronomical Society of the Pacific Conference Series, Difmap: an Interactive Program for Synthesis Imaging.* p. 77
- Unwin S. C., Wehrle A. E., Lobanov A. P., Zensus J. A., Madejski G. M., Aller M. F., Aller H. D., 1997, *The Astrophysical Journal*, 480, 596
- Vlahakis N., Königl A., 2004, *ApJ*, 605, 656
- Walker R. C., Dhawan V., Romney J. D., Kellermann K. I., Vermeulen R. C., 2000, *The Astrophysical Journal*, 530, 233
- Wardle J. F. C., Homan D. C., Ojha R., Roberts D. H., 1998, *Nature*, 395, 457
- Woo J.-H., Urry C. M., 2002, *The Astrophysical Journal*, 579, 530
- Wu Z., Gu M., Jiang D., 2009, *Research in Astronomy and Astrophysics*, 9, 168
- Zenitani S., Hoshino M., 2008, *ApJ*, 677, 530

This paper has been typeset from a $\text{\TeX}/\text{\LaTeX}$ file prepared by the author.

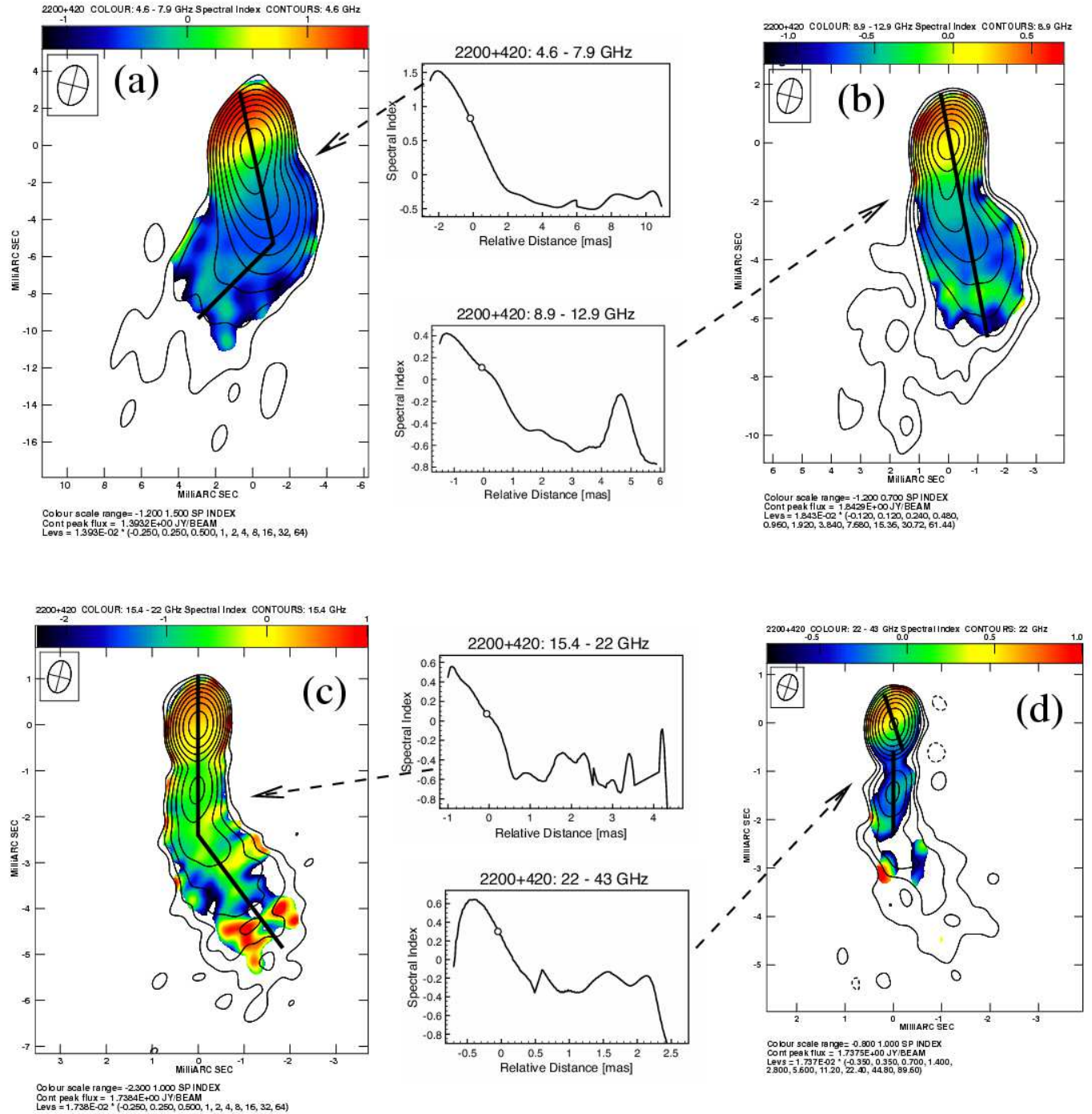


Figure 1. Spectral index maps for 2200+420 constructed from frequency pairs, with plots of slices along the jet region indicated by the solid line. (a) 4.6–7.9 GHz. Spectral index scale range: -1.2 to 1.5 . Clip levels of I maps: 3.5 mJy (4.6 GHz), 3.8 mJy (7.9 GHz). Beam FWHM and Position Angle: 2.17×1.60 mas, -14° (4.6 GHz). Contours: 4.6 GHz I , starting at 3.48 mJy and increasing by factors of 2. (b) 8.9–12.9 GHz. Spectral index scale range: -1.2 to 0.7 . Clip levels of I maps: 2.2 mJy (8.9 GHz), 6.8 mJy (12.9 GHz). Beam FWHM and Position Angle: 1.21×0.84 mas, -14° (8.9 GHz). Contours: 8.9 GHz I , starting at 2.21 mJy and increasing by factors of 2. (c) 15.4–22 GHz. Spectral index scale range: -2.3 to 1.0 . Clip levels of I maps: 5.2 mJy (15.4 GHz), 5.9 mJy (22 GHz). Beam FWHM and Position Angle: 0.71×0.49 mas, -14° (15.4 GHz). Contours: 15.4 GHz I , starting at 4.35 mJy and increasing by factors of 2. (d) 22–43 GHz. Spectral index scale range: -0.8 to 1.0 . Clip levels of I maps: 6.9 mJy (22 GHz), 13.3 mJy (43 GHz). Beam FWHM and Position Angle: 0.55×0.40 mas, -19° (22 GHz). Contours: 22 GHz I , starting at 6.08 mJy and increasing by factors of 2. The arrows connect the plots of the spectral index slices to their corresponding maps. The hollow circle on the slice plot indicates the core position at the lower frequency of the pair.

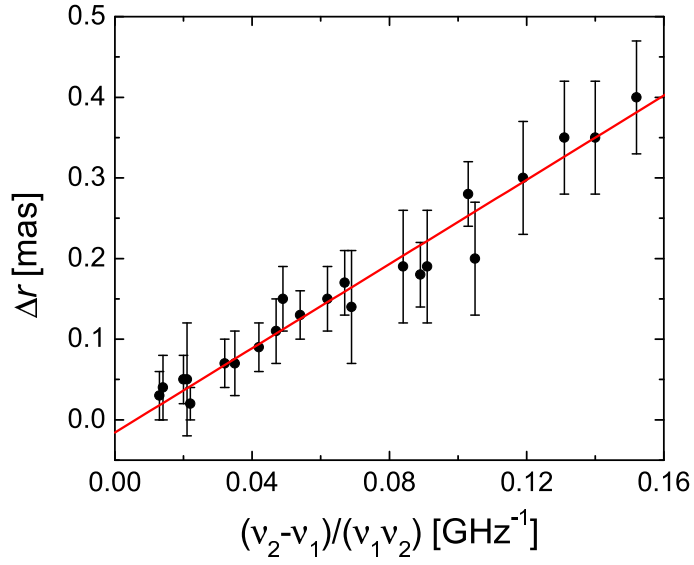


Figure 2. Straight-line fit to the all the core-shift data for 2200+420, assuming equipartition. The y-intercept value is equal to -0.01 ± 0.01 mas. A straight-line fit through the origin is expected for $k_r = 1$.

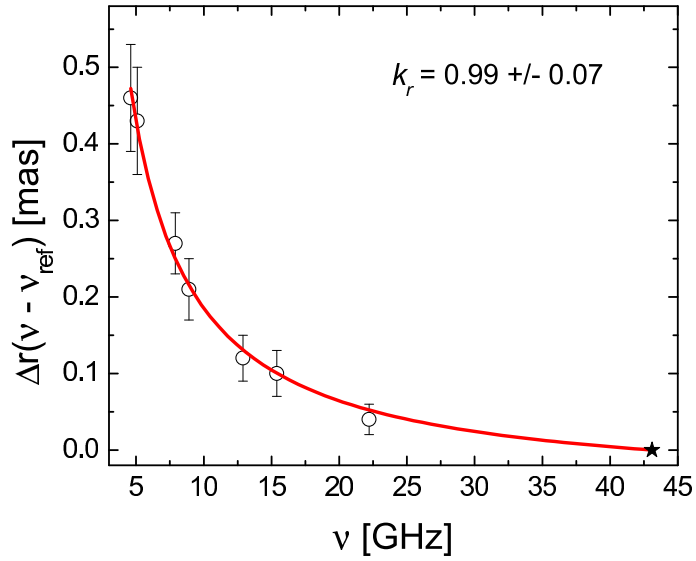


Figure 3. Plot of core-shift measurements versus frequency for 2200+420 (listed in Table 3), using 43 GHz as the reference frequency. Best-fit line: $\Delta r = A(\nu^{-1/k_r} - 43.1^{-1/k_r})$ with parameters $A = 2.5 \pm 0.3$ and $k_r = 0.99 \pm 0.07$

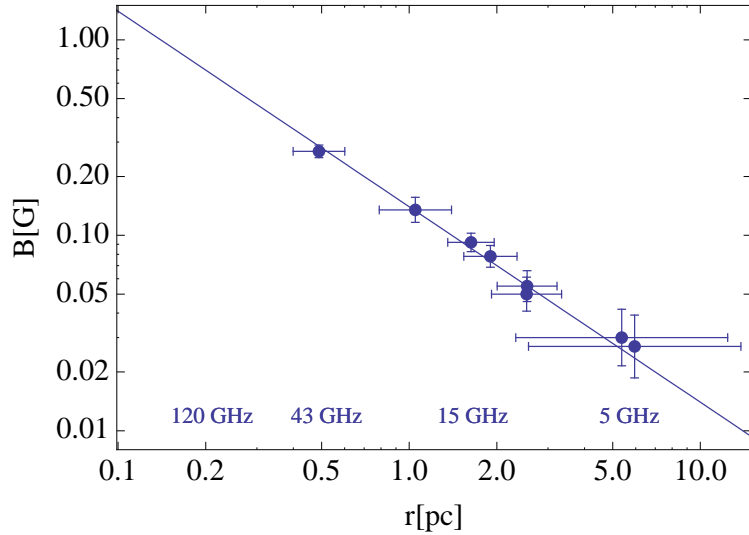


Figure 4. Plot of magnetic field strength (B) in units of Gauss versus distance along the jet (r) in units of parsecs for the core of 2200+420 at 4.6, 5.1, 7.9, 8.9, 12.9, 15.4, 22.2 & 43 GHz using $k_r = 1$. Also plotted is the best-fit line $B = B_1 r^{-1}$ with $B_1 = 0.139$ G with a formal error of 0.006 G.

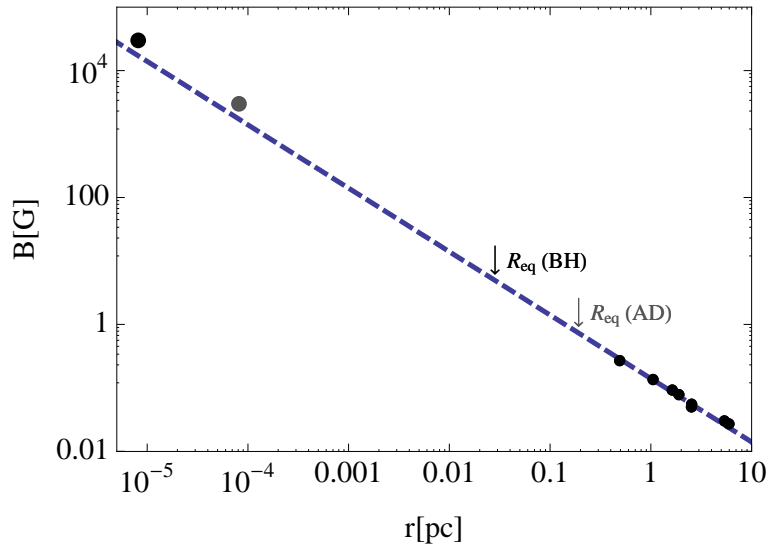


Figure 5. Extended plot of B versus r for 2200+420 to include the extrapolated magnetic field strength ($B \simeq 0.14 r^{-1}$) at the accretion disk ($10r_g$) and black holes (r_g) distances. The estimated equipartition radii from K07 are indicated by the arrows with $R_{\text{eq,AD}} \sim 0.2$ pc and $R_{\text{eq,BH}} \sim 0.03$ pc. Also plotted are points at $10r_g$ (grey) and r_g (black) representing the theoretically expected magnetic field strengths for a magnetically powered jet.

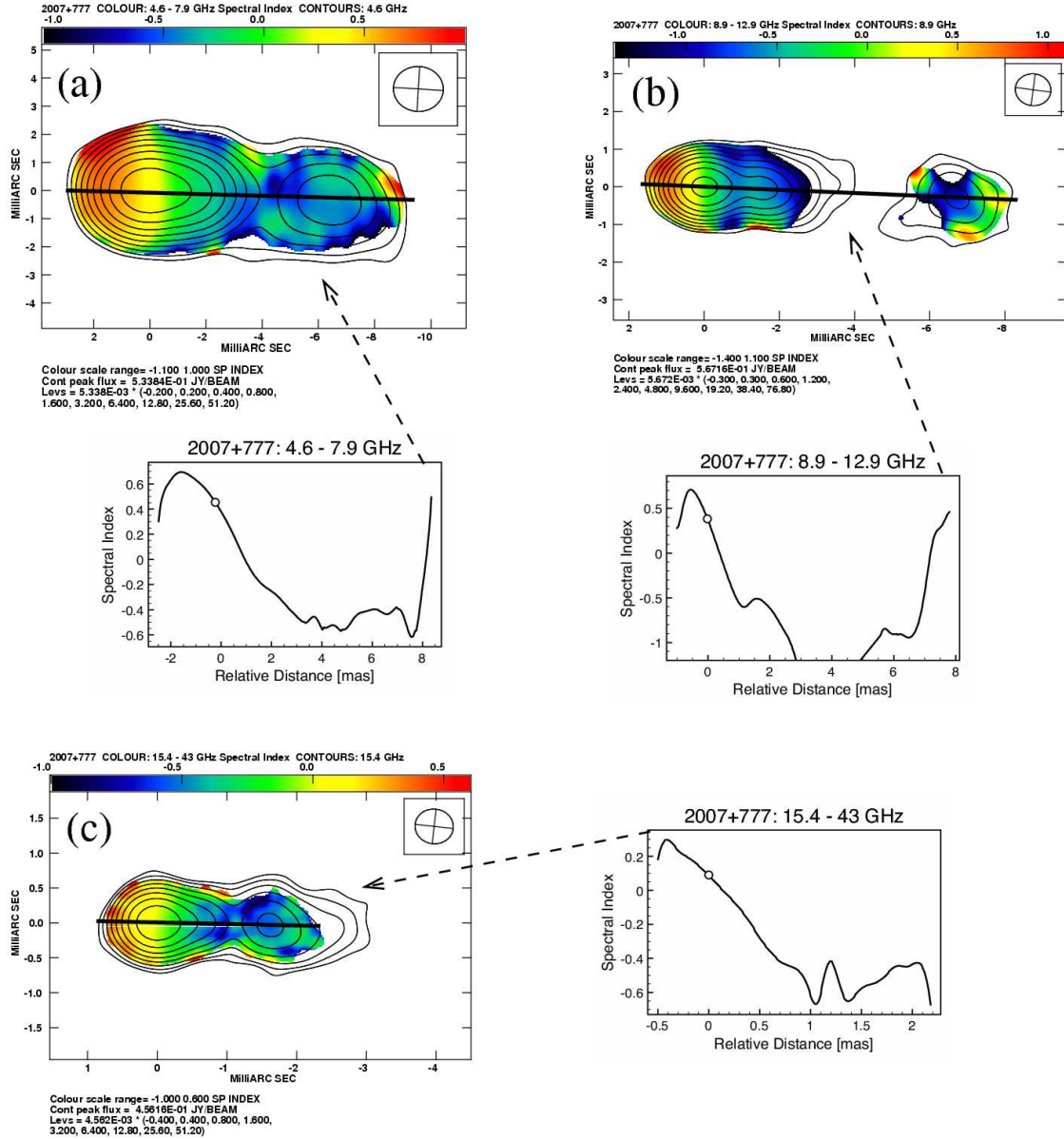


Figure 6. Spectral index maps for 2007+777 constructed from frequency pairs, with plots of slices along the jet region indicated by the solid line. (a) 4.6–7.9 GHz. Spectral index scale range: -1.1 to 1.0 . Clip levels of I maps: 1.1 mJy (4.6 GHz), 2.0 mJy (7.9 GHz). Beam FWHM and Position Angle: 1.78×1.60 mas, 86.5° (4.6 GHz). Contours: 4.6 GHz I , starting at 1.07 mJy and increasing by factors of 2. (b) 8.9–12.9 GHz. Spectral index scale range: -1.4 to 1.1 . Clip levels of I maps: 1.7 mJy (8.9 GHz), 2.3 mJy (12.9 GHz). Beam FWHM and Position Angle: 0.95×0.84 mas, 82.5° (8.9 GHz). Contours: 8.9 GHz I , starting at 1.70 mJy and increasing by factors of 2. (c) 15.4–43 GHz. Spectral index scale range: -1 to 0.6 . Clip levels of I maps: 1.8 mJy (15.4 GHz), 7.7 mJy (43 GHz). Beam FWHM and Position Angle: 0.55×0.50 mas, 83.6° (15.4 GHz). Contours: 15.4 GHz I , starting at 1.82 mJy and increasing by factors of 2. The arrows connect the plots of the spectral index slices to their corresponding maps. The hollow circle on the slice plot indicates the core position at the lower frequency of the pair.

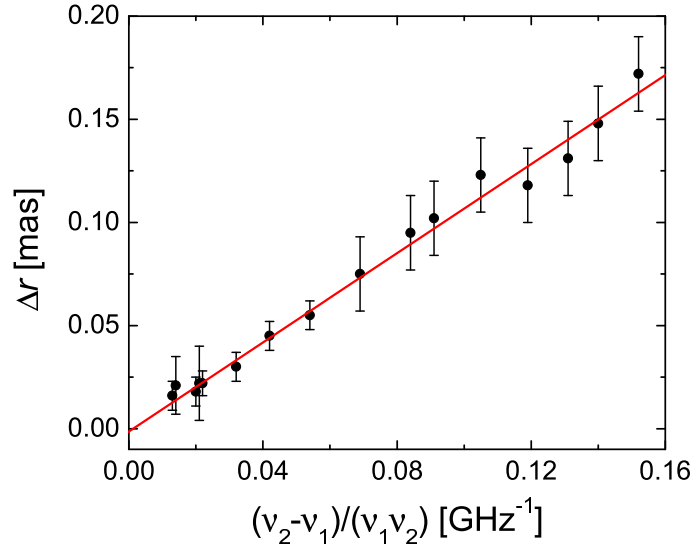


Figure 7. Straight-line fit to the all the core-shift data for 2007+777, assuming equipartition. The y-intercept value is equal to -0.001 ± 0.004 mas. A straight-line fit through the origin is expected for $k_r = 1$.

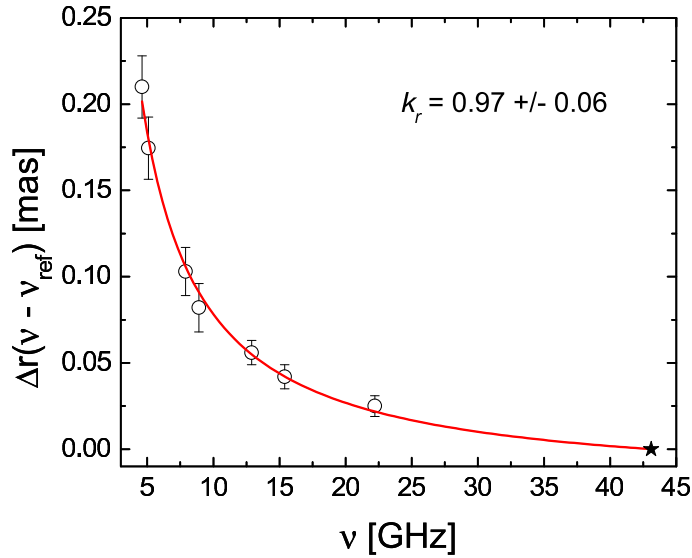


Figure 8. Plot of core-shift measurements versus frequency for 2007+777 (listed in Table 6), using 43 GHz as the reference frequency. Best-fit line: $\Delta r = A(\nu^{-1/k_r} - 43.1^{-1/k_r})$ with parameters $A = 1.08 \pm 0.11$ and $k_r = 0.97 \pm 0.06$

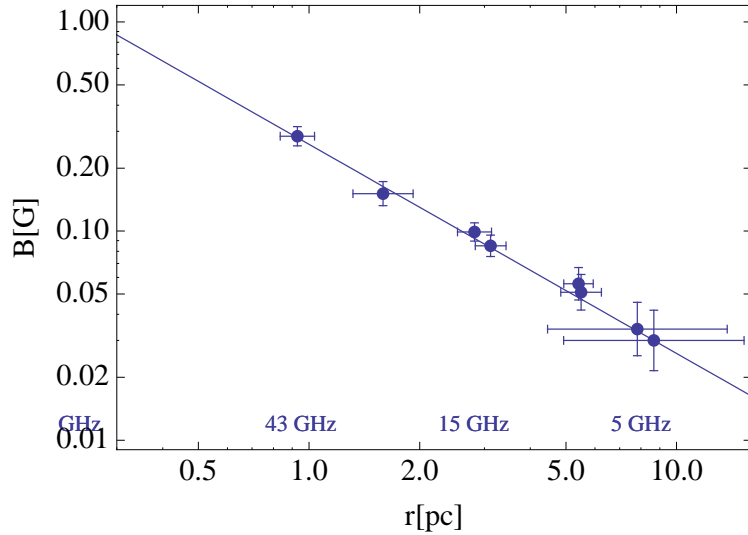


Figure 9. Plot of magnetic field strength (B) in units of Gauss versus distance along the jet (r) in units of parsecs for the core of 2007+777 at 4.6, 5.1, 7.9, 8.9, 12.9, 15.4, 22.2 & 43 GHz using $k_r = 1$. Also plotted is the best-fit line $B = B_1 r^{-1}$ with $B_1 = 0.257$ G with a formal error of 0.007 G.

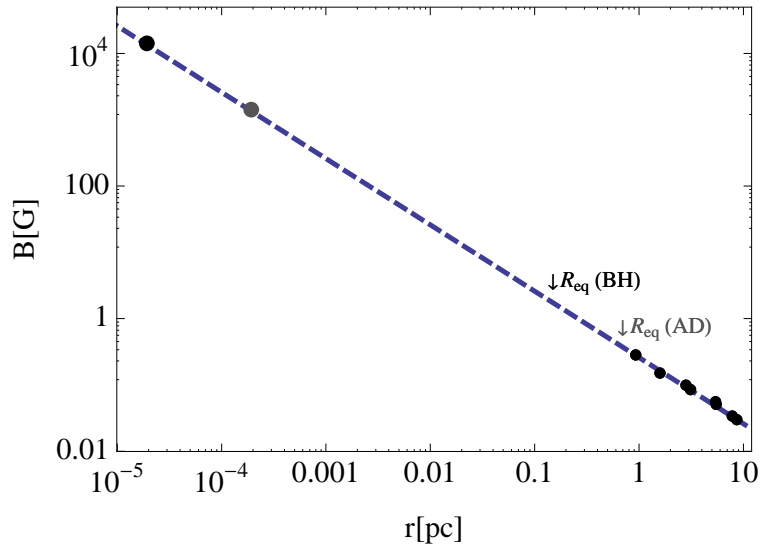


Figure 10. Extended plot of B versus r for 2007+777 to include the extrapolated magnetic field strength ($B \simeq 0.26r^{-1}$) at the accretion disk ($10r_g$) and black holes (r_g) distances. The estimated equipartition radii from the model K07 are indicated by the arrows with $R_{\text{eq,AD}} \sim 0.7$ pc and $R_{\text{eq,BH}} \sim 0.1$ pc. Also plotted are points at $10r_g$ (grey) and r_g (black) representing the theoretically expected magnetic field strengths for a magnetically powered jet.

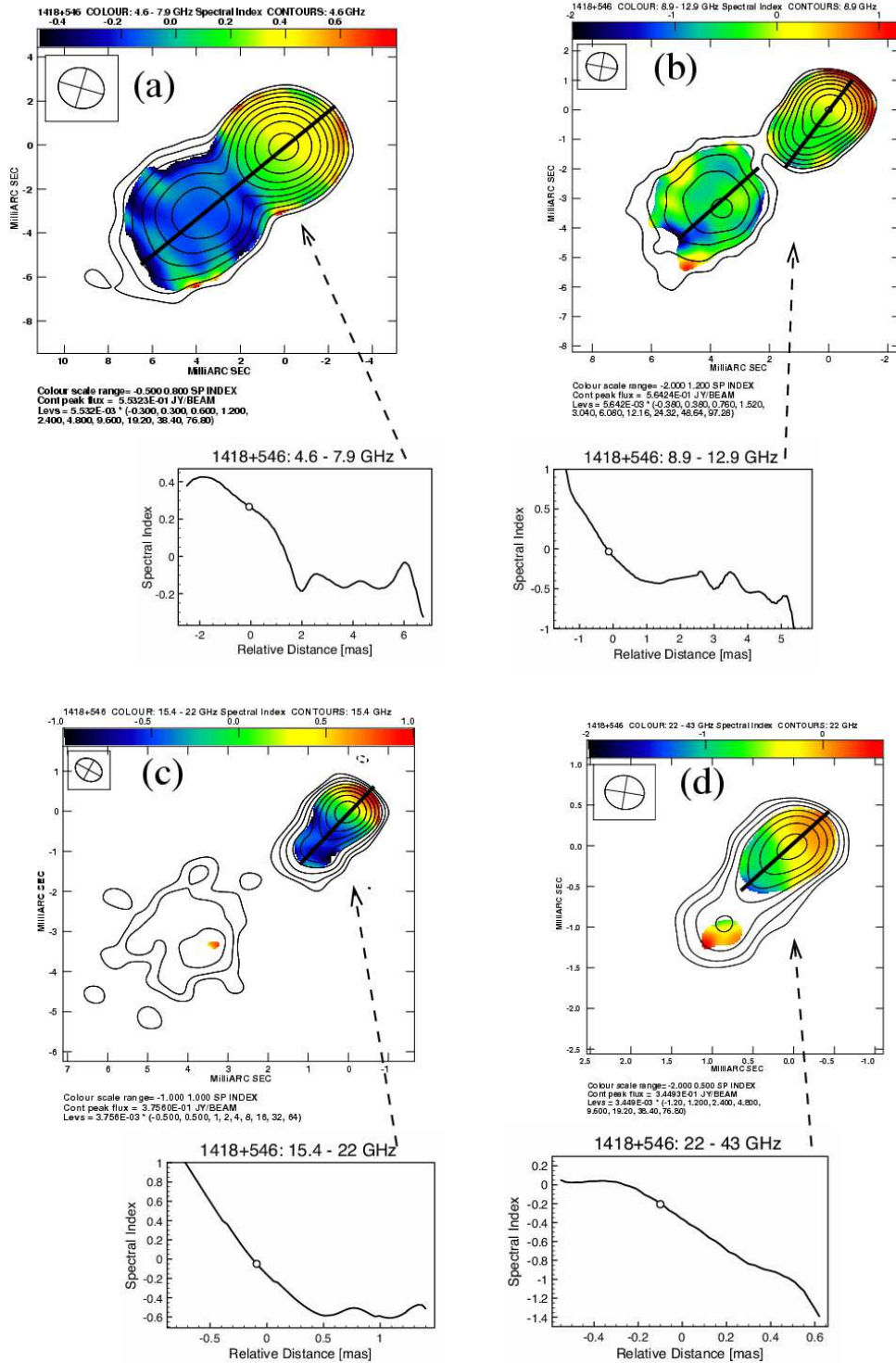


Figure 11. Spectral index maps for 1418+546 constructed from frequency pairs, with plots of slices along the jet region indicated by the solid line. (a) 4.6–7.9 GHz. Spectral index scale range: -0.5 to 0.8 . Clip levels of I maps: 1.7 mJy (4.6 GHz), 2.6 mJy (7.9 GHz). Beam FWHM and Position Angle: 2.10×1.84 mas, 73.6° (4.6 GHz). Contours: 4.6 GHz I , starting at 1.66 mJy and increasing by factors of 2. (b) 8.9–12.9 GHz. Spectral index scale range: -2 to 1.2 . Clip levels of I maps: 2.1 mJy (8.9 GHz), 3.7 mJy (12.9 GHz). Beam FWHM and Position Angle: 1.06×0.94 mas, 79.6° (8.9 GHz). Contours: 8.9 GHz I , starting at 2.14 mJy and increasing by factors of 2. (c) 15.4–22 GHz. Spectral index scale range: -1.0 to 1.0 . Clip levels of I maps: 3.0 mJy (15.4 GHz), 5.8 mJy (22 GHz). Beam FWHM and Position Angle: 0.69×0.54 mas, 61.9° (15.4 GHz). Contours: 15.4 GHz I , starting at 1.88 mJy and increasing by factors of 2. (d) 22–43 GHz. Spectral index scale range: -2.0 to 0.5 . Clip levels of I maps: 4.2 mJy (22 GHz), 9.2 mJy (43 GHz). Beam FWHM and Position Angle: 0.48×0.42 mas, 80.8° (22 GHz). Contours: 22 GHz I , starting at 4.14 mJy and increasing by factors of 2. The arrows connect the plots of the spectral index slices to their corresponding maps. The hollow circle on the slice plot indicates the core position at the lower frequency of the pair.

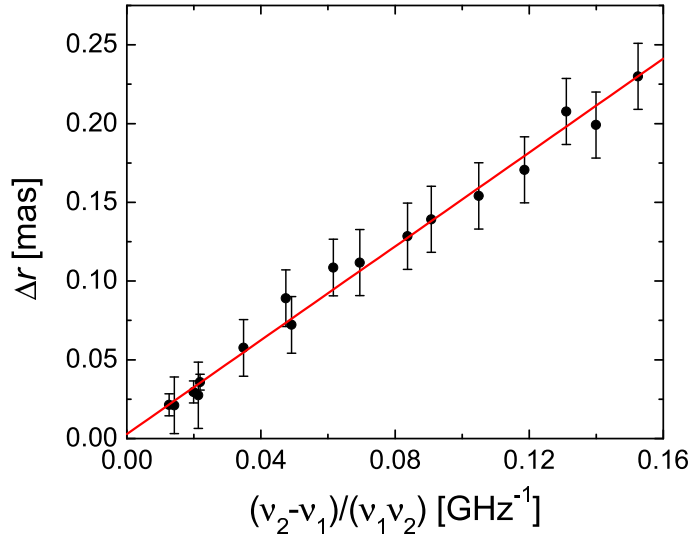


Figure 12. Straight-line fit to the all the core-shift data for 1418+546, assuming equipartition. The y-intercept value is equal to 0.003 ± 0.004 mas. A straight-line fit through the origin is expected for $k_r = 1$.

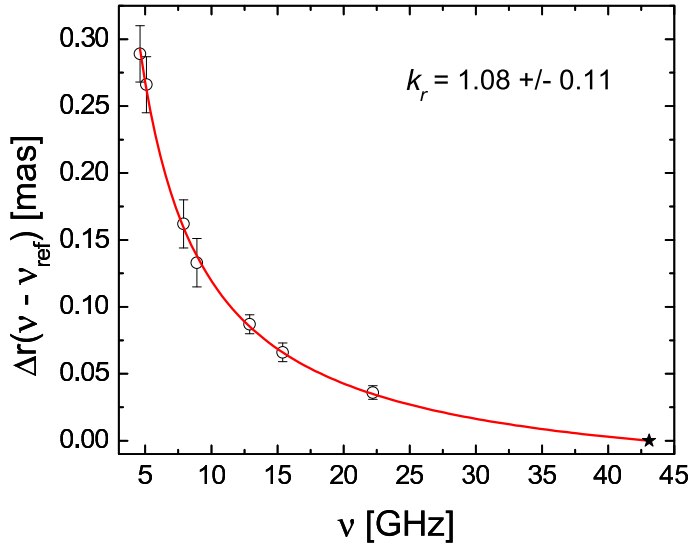


Figure 13. Plot of core-shift measurements versus frequency for 1418+546 (listed in Table 13), using 43 GHz as the reference frequency. Best-fit line: $\Delta r = A(\nu^{-1/k_r} - 43.1^{-1/k_r})$ with parameters $A = 1.4 \pm 0.2$ and $k_r = 1.08 \pm 0.11$

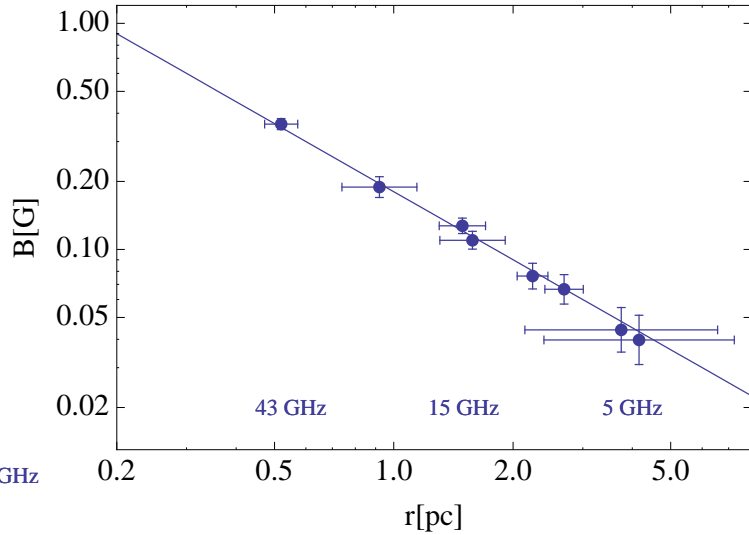


Figure 14. Plot of magnetic field strength (B) in units of Gauss versus distance along the jet (r) in units of parsecs for the core of 1418+546 at 4.6, 5.1, 7.9, 8.9, 12.9, 15.4, 22.2 & 43 GHz using $k_r = 1$. Also plotted is the best-fit line $B = B_1 r^{-1}$ with $B_1 = 0.178$ G with a formal error of 0.006 G.

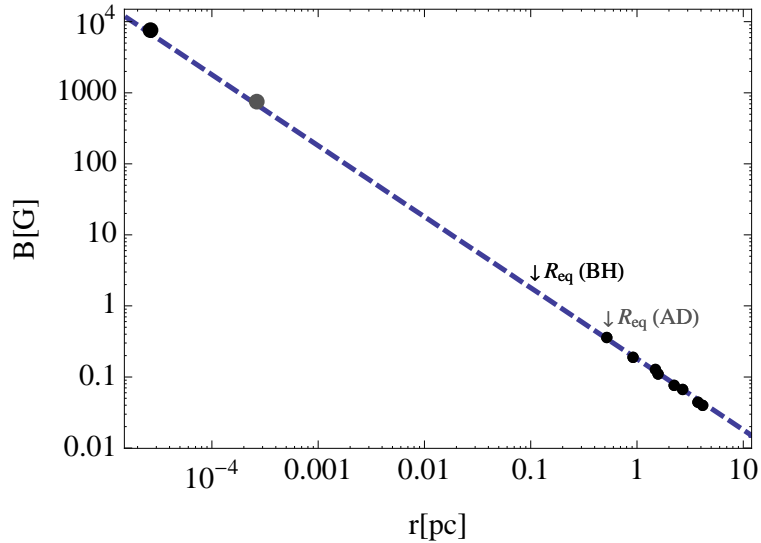


Figure 15. Extended plot of B versus r for 1418+546 to include the extrapolated magnetic field strength ($B \simeq 0.18 r^{-1}$) at the accretion disk ($10r_g$) and black holes (r_g) distances. The estimated equipartition radii from the model K07 are indicated by the arrows with $R_{\text{eq,AD}} \sim 0.5$ pc and $R_{\text{eq,BH}} \sim 0.1$ pc. Also plotted are points at $10r_g$ (grey) and r_g (black) representing the theoretically expected magnetic field strengths for a magnetically powered jet.

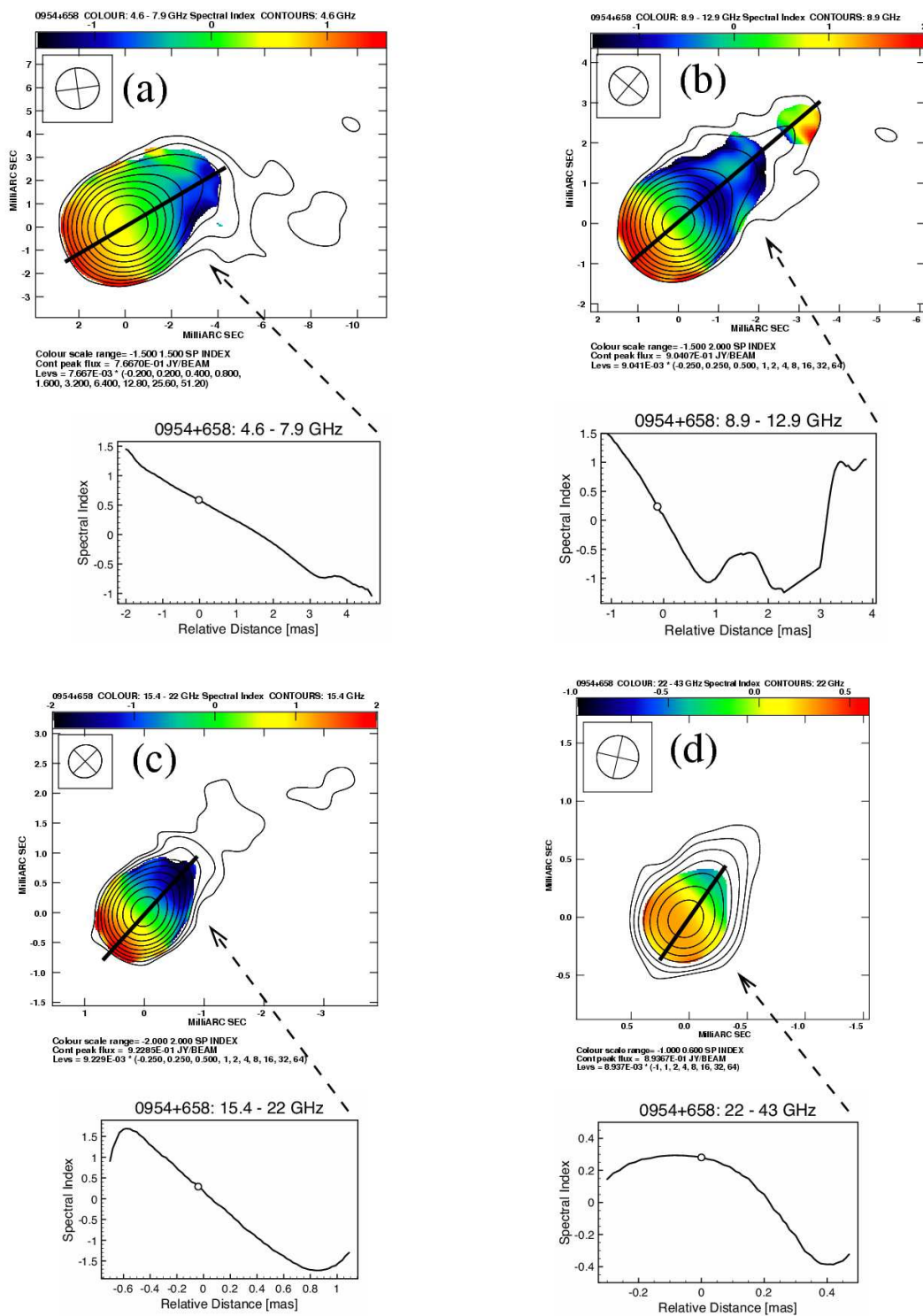


Figure 16. Spectral index maps for 0954+658 constructed from frequency pairs, with plots of slices along the jet region indicated by the solid line. (a) 4.6–7.9 GHz. Spectral index scale range: -1.5 to 1.5 . Clip levels of I maps: 1.5 mJy (4.6 GHz), 3.8 mJy (7.9 GHz). Beam FWHM and Position Angle: 1.87×1.76 mas, -82.4° (4.6 GHz). Contours: 4.6 GHz I , starting at 1.53 mJy and increasing by factors of 2. (b) 8.9–12.9 GHz. Spectral index scale range: -1.5 to 2.0 . Clip levels of I maps: 2.3 mJy (8.9 GHz), 2.6 mJy (12.9 GHz). Beam FWHM and Position Angle: 0.98×0.95 mas, 49.8° (8.9 GHz). Contours: 8.9 GHz I , starting at 2.26 mJy and increasing by factors of 2. (c) 15.4–22 GHz. Spectral index scale range: -2.0 to 2.0 . Clip levels of I maps: 2.8 mJy (15.4 GHz), 7.8 mJy (22 GHz). Beam FWHM and Position Angle: 0.57×0.54 mas, -45.5° (15.4 GHz). Contours: 15.4 GHz I , starting at 2.31 mJy and increasing by factors of 2. (d) 22–43 GHz. Spectral index scale range: -1.0 to 0.6 . Clip levels of I maps: 8.9 mJy (22 GHz), 16.0 mJy (43 GHz). Beam FWHM and Position Angle: 0.37×0.36 mas, -12.9° (22 GHz). Contours: 22 GHz I , starting at 8.94 mJy and increasing by factors of 2. The arrows connect the plots of the spectral index slices to their corresponding maps. The hollow circle on the slice plot indicates the core position at the lower frequency of the pair.

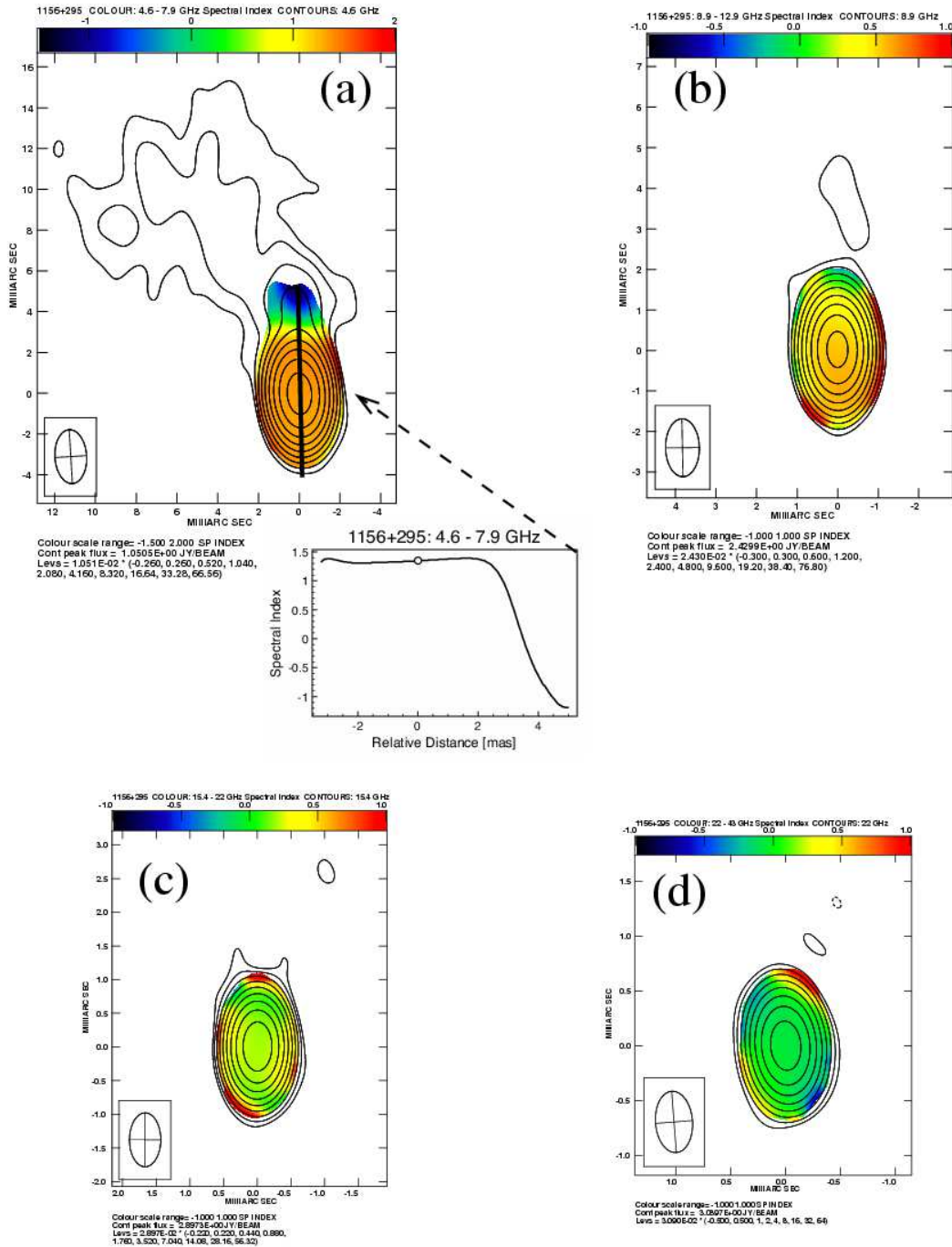


Figure 17. Spectral index maps for 1156+295 constructed from frequency pairs, with a plot of a slice along the 4.6–7.9 GHz map indicated by the solid line. (a) 4.6–7.9 GHz. Spectral index scale range: -1.5 to 2.0 . Clip levels of I maps: 2.7 mJy (4.6 GHz), 10.9 mJy (7.9 GHz). Beam FWHM and Position Angle: 2.65×1.56 mas, 3.5° (4.6 GHz). Contours: 4.6 GHz I , starting at 2.73 mJy and increasing by factors of 2. (b) 8.9–12.9 GHz. Spectral index scale range: -1.0 to 1.0 . Clip levels of I maps: 7.3 mJy (8.9 GHz), 14.9 mJy (12.9 GHz). Beam FWHM and Position Angle: 1.43×0.83 mas, 1.1° (8.9 GHz). Contours: 8.9 GHz I , starting at 7.29 mJy and increasing by factors of 2. (c) 15.4–22 GHz. Spectral index scale range: -1.0 to 1.0 . Clip levels of I maps: 5.8 mJy (15.4 GHz), 24.9 mJy (22 GHz). Beam FWHM and Position Angle: 0.80×0.47 mas, -0.3° (15.4 GHz). Contours: 15.4 GHz I , starting at 6.37 mJy and increasing by factors of 2. (d) 22–43 GHz. Spectral index scale range: -1.0 to 1.0 . Clip levels of I maps: 15.5 mJy (22 GHz), 44.2 mJy (43 GHz). Beam FWHM and Position Angle: 0.56×0.34 mas, 4.4° (22 GHz). Contours: 22 GHz I , starting at 15.45 mJy and increasing by factors of 2.

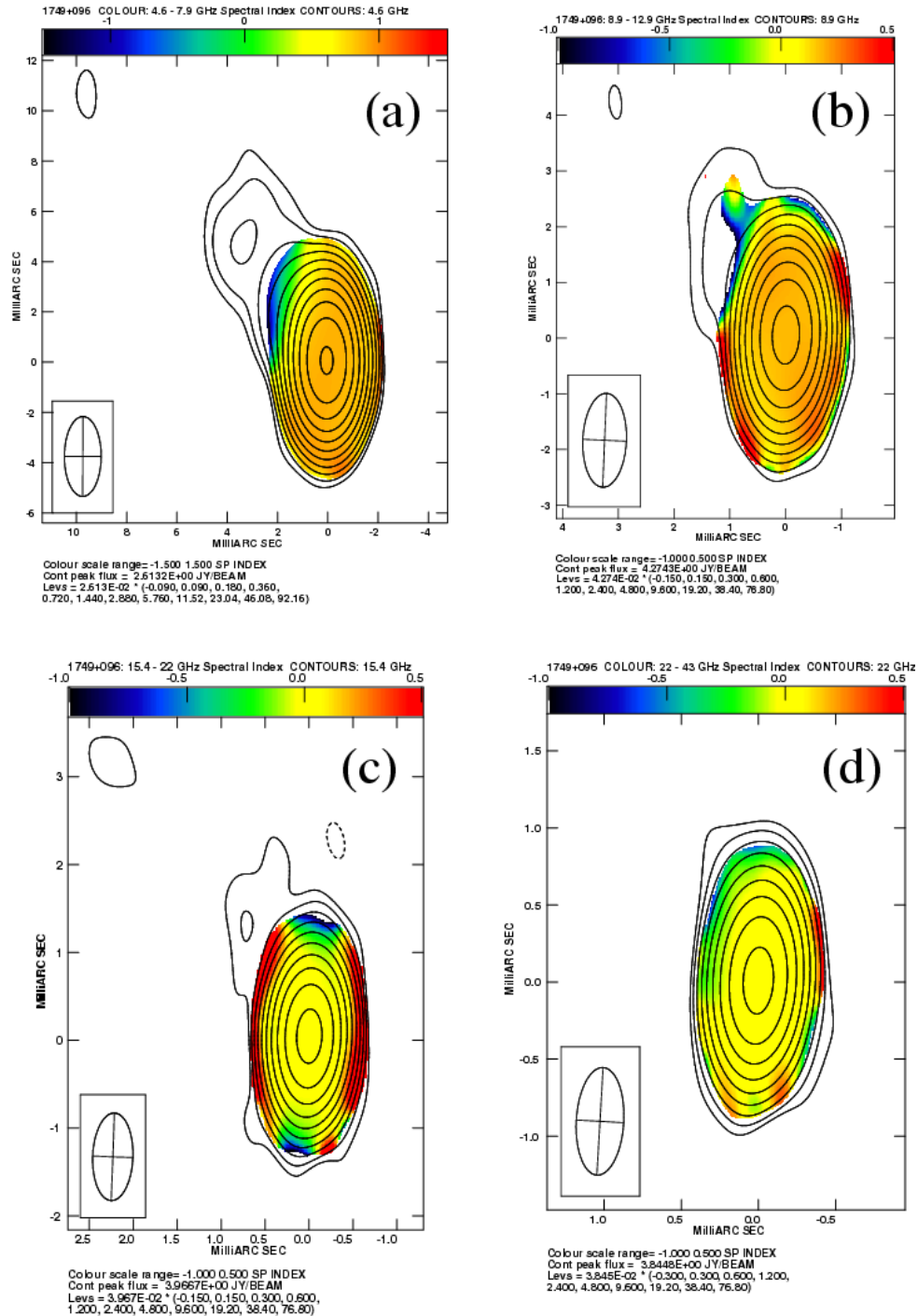


Figure 18. Spectral index maps for 1749+096 constructed from frequency pairs. (a) 4.6–7.9 GHz. Spectral index scale range: -1.5 to 1.5 . Clip levels of I maps: 2.4 mJy (4.6 GHz), 8.4 mJy (7.9 GHz). Beam FWHM and Position Angle: 3.18×1.46 mas, -0.3° (4.6 GHz). Contours: 4.6 GHz I , starting at 2.35 mJy and increasing by factors of 2. (b) 8.9–12.9 GHz. Spectral index scale range: -1.0 to 0.5 . Clip levels of I maps: 6.4 mJy (8.9 GHz), 9.1 mJy (12.9 GHz). Beam FWHM and Position Angle: 1.69×0.78 mas, -2.4° (8.9 GHz). Contours: 8.9 GHz I , starting at 6.41 mJy and increasing by factors of 2. (c) 15.4–22 GHz. Spectral index scale range: -1.0 to 0.5 . Clip levels of I maps: 8.3 mJy (15.4 GHz), 15.7 mJy (22 GHz). Beam FWHM and Position Angle: 1.00×0.46 mas, -2.2° (15.4 GHz). Contours: 15.4 GHz I , starting at 5.95 mJy and increasing by factors of 2. (d) 22–43 GHz. Spectral index scale range: -1.0 to 0.5 . Clip levels of I maps: 11.5 mJy (22 GHz), 39.3 mJy (43 GHz). Beam FWHM and Position Angle: 0.70×0.31 mas, -3.3° (22 GHz). Contours: 22 GHz I , starting at 11.54 mJy and increasing by factors of 2.